LUNAR CRATER ORIGIN IN THE MARIA FROM ANALYSIS OF ORBITER PHOTOGRAPHS

By G. FIELDER,† R. J. FRYER,† C. TITULAER, A. K. HERRING and B. WISE
Lunar and Planetary Laboratory, University of Arizona

(*Communicated by S. K. Runcorn, F.R.S.—Received* 26 *January* 1970—*Revised* 5 *February* 1971)

[Plates 5 to 7]

CONTENTS

One third of a million counts on 73 127 craters in 22 test areas of lunabase (the dark areas of the Moon, normally maria) have been made with the aim of diagnosing the origin of the craters that are predominantly between 100 and 2000 m in diameter by the use of a statistical method that is capable of measuring both the chaining and clustering of craters. Independent measurements of clustering have been made using photometry and using equi-areal counts to determine the number density of craters. It is argued that craters with alined centres that trend in parallel directions over vast distances are exclusively of internal origin. Strong evidence that a high proportion of the chains are of tectonic origin is found. Other criteria, such as a systematic change in the number density of craters over a test area or an excess of craters on a recent lava flow, are also used to argue for endogenic craters. Computer simulations of random fields of craters and of specially proportioned linear arrays and clusters of craters on random backgrounds have been used widely in the interpretation of the observations. By comparing the results of statistical tests on the real distributions of crater centres with those on the distributions created by computer it has been possible to set probable limits on the number of endogenic craters in each test area.

† Present address: Lunar and Planetary Unit, Department of Environmental Sciences, University of Lancaster, Bailrigg, Lancaster.

Vol. 271. A. 1215 (Price £1.50; U.S. $3.90) 31 [Published 27 January 1972

Because the method is statistical, results for individual areas will embody unknown errors. Averages, taking several areas at a time, are more meaningful. Using all the data together, we find that at least 33 %, but not more than 51 %, of the craters sampled are of endogenic origin.

It is shown that the flux of meteoroids has not necessarily varied for the past few thousand million years.

1. Introduction

Circumstantial evidence in favour of the meteoric origin of many of the lunar craters is strong. In addition, most authorities deduce that a certain proportion of the craters are of internal origin. Attempts to put limits on the number of impact and endogenic craters were made by Kuiper (1965), Fielder (1965, 1966), McCauley (1967), Hartmann (1967) and Chapman (1968) and their estimates are listed in table 1.

Table 1. Qualitative estimates of the proportion of lunar craters formed internally

author	method	crater size km	crater percentages internal	crater percentages impact
Kuiper (1965)	morphology of craters in Alphonsus	0.1 to 3	80 to 90	10 to 20
Fielder (1965)	asteroidal and lunar crater counts	>6	90	10
Fielder (1966)	chaining of craters in Ptolemaeus	1.5 to 4	$\geqslant 40$	$\leqslant 60$
McCauley (1967)	morphology and stratigraphy of craters in Alphonsus	0.1 to 3	$\geqslant 25$	$\geqslant 25$
Hartmann (1967)	crater counts on Alphonsus floor, using counts on walls as control	0.1 to 3	67	33
Chapman (1968)	chaining of craters and counts as a function of crater type, using *Ranger* data	0.3 to 1	$\geqslant 50$	$\leqslant 50$

Clearly there is need to specify more accurately the proportion of craters of different genesis in different lunar regions; only after the endogenic craters and secondary impact craters are specified, for a given region, can the number of primary impact craters be determined; and only then can counts of craters be used in an attempt to date that region through use of the influx law of meteoric material. Our chief aim in this paper is to perform such a separation for craters in the maria. Use of high-quality *Lunar Orbiter* photographs ensured that craters from 100 m in diameter, in the area of largest scale, and from 703 m in diameter, in the area of smallest scale, could be recorded without significant observational losses. In one case only we used a U.S.A.F. map as the source of data.

A newly devised statistical approach to the problem is used here to set limits to the number of craters of (*a*) primary impact, (*b*) endogenic origin. Basically, we adapt the index of dispersion test or 'V test' of Fielder & Marcus (1967) to our requirements. This is a very sensitive test for alinements of crater centres, but also detects clustering of centres.

In the mare areas under investigation, the crater densities (numbers of craters per unit area) are low and obliteration through overlapping does not introduce any sensible departure from randomness.† The mean size of the craters studied in this investigation is of the order of 1 km, and the complete range of size is from 100 m to 26 km. Since there are few craters larger than the 10 km size in any area selected for study, the upper limit of 26 km is not representative of the diameters studied; most of the craters lie between 100 and 2000 m in diameter.

† This is demonstrated in §3.

The interpretation of the *V*-tests on each 'test area' listed in table 2 has been strictly controlled by recourse to a similar test on a 'control map' of craters having the same crater density as that of the test area. However, each control map differs from the map of the corresponding test area in such a way that the centres of craters on the control map are arranged at random with the exception that a known proportion of the centres is arranged in linear chains, the chains themselves having random separations but the craters in a chain having a fixed separation measured by the 'separation index'. Furthermore, we generate several control maps, each with a different separation index, for each test area. The nature and degree of alinement of craters and the amount to which they cluster over and above that found for the control population may then be determined, between limits, from the *V*-tests.

We also present auxiliary studies of the clustering behaviour of craters by a photometric method. There is no doubt that the craters in the range of size considered are distributed neither uniformly nor randomly across the Moon's surface.

2. Counts of craters

2.1. *Mapping craters*

Four problems arise in studying the distribution of lunar crater centres and sizes: (i) incompleteness of observation; (ii) obliteration of smaller craters by relatively recent, large craters; (iii) the fact that craters display a range of types, from the sharply sculptured 'eumorphic' type to the soft 'submorphic' type; and (iv) the difficulty in measuring unambiguously the 'true' diameter of a crater from a photograph.

Incompleteness of observation, a function of the resolution attained in a given photograph, may be reduced by truncating counts at a certain minimum diameter of craters. In the majority of the regions studied we found this diameter to be no more than 1 mm of photographic print, corresponding to between 100 and 703 m of lunar surface, depending on the scale of the photograph. In one test region, Flamsteed P, counts were made by G.F. down to 0.25 mm; but were thought to be nearly complete only down to $\frac{1}{2}$ mm, corresponding to 258 m of lunar surface. Even so, great care had to be taken to ensure this degree of completeness and, judged against the extra numbers of craters gained, the time of counting was increased disproportionately. The size of crater at which counts were truncated was determined in two ways: different observers counted the same region and their results were compared; and graphs relating numbers to diameters were examined for changes of slope peculiar to the end corresponding to small diameters. The results of the different observers and the nature and form of the graphs will be discussed in § 2.2.

The problem of obliteration of smaller craters by relatively recent large craters has been discussed by Marcus (1966*a*, *b*) and others. First, in order to minimize the effect, we chose regions in the maria where the crater density was low. Secondly, in general we selected the regions so as to avoid very large craters. With these conditions, counts of numbers of craters in set diameter increments were made and the same data were fed to a computer and re-represented as circles with randomly placed centres. The loss of craters through overlapping was found to be negligible in all cases (§ 2.2).

The separation of craters into different types was deliberately avoided in all areas except one. In the case of Sinus Medii, where counts were made down to the 116 m diameter, exceptionally

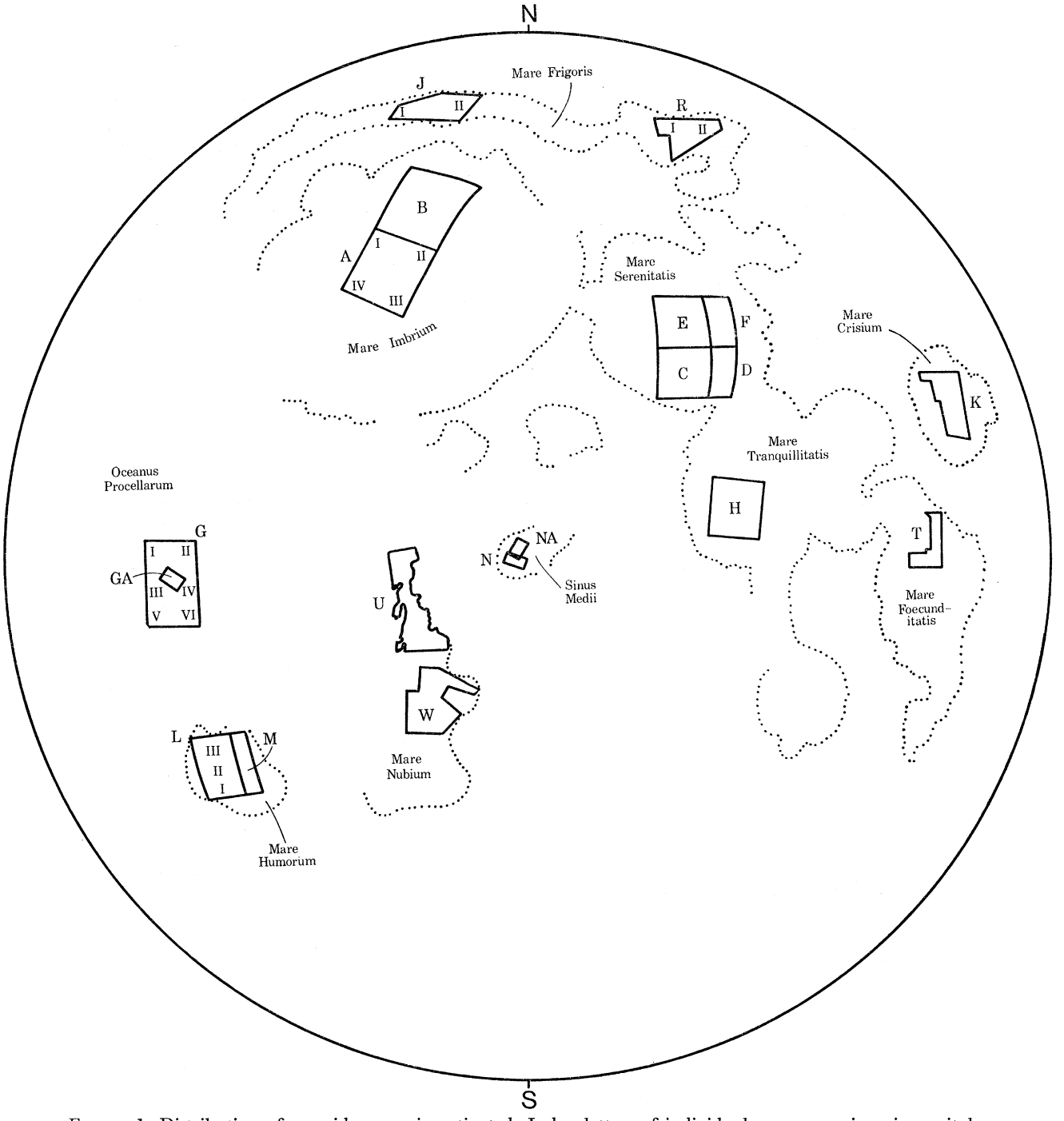

FIGURE 1. Distribution of nearside areas investigated. Index letters of individual areas are given in capitals. Subdivisions are given in roman numerals. Dotted curves show approximate mare boundaries. (Moon–orthographic projection.)

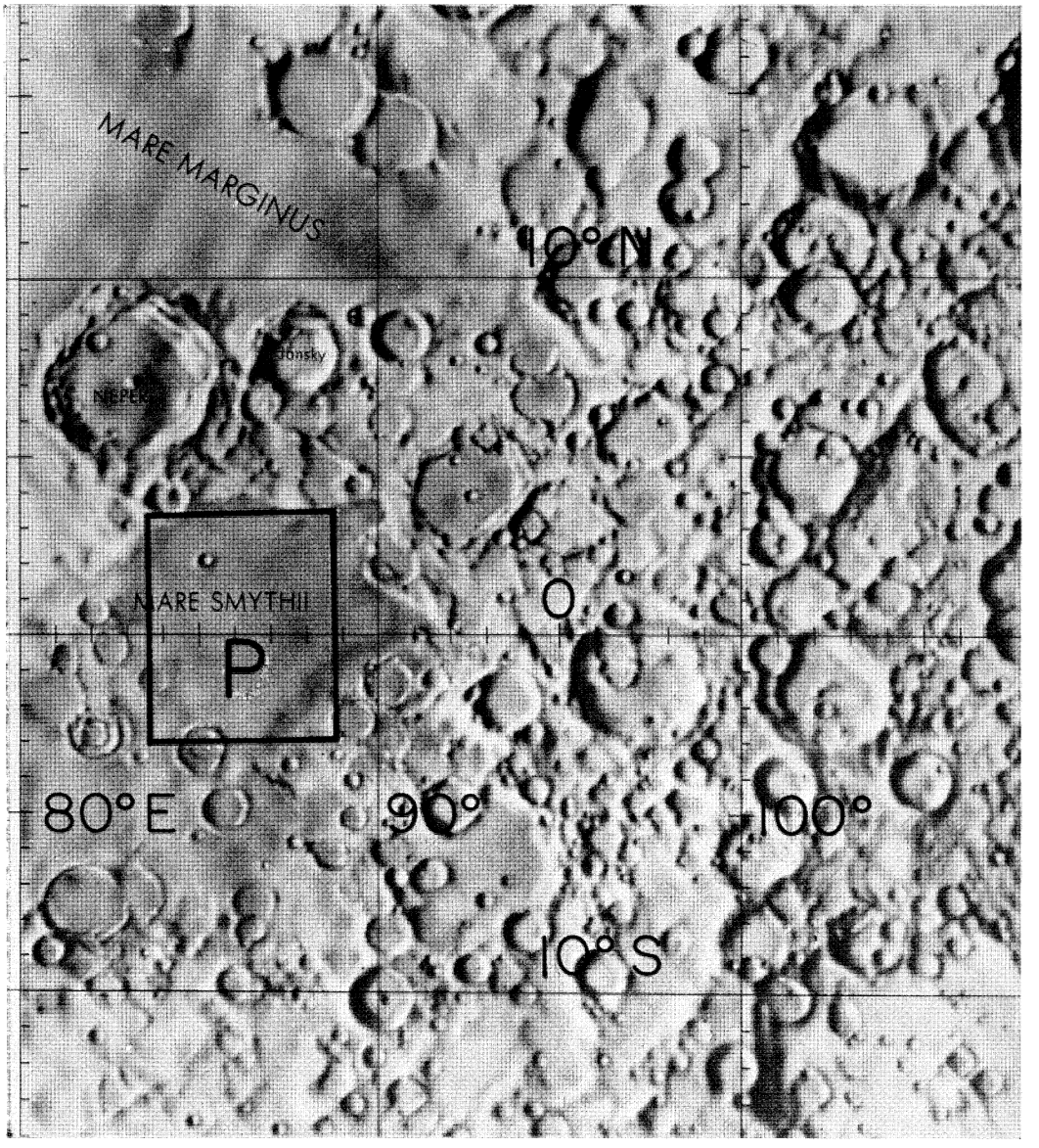

FIGURE 2. Extent of 'area P' in Mare Smythii (limb area).

(*Facing p.* 364)

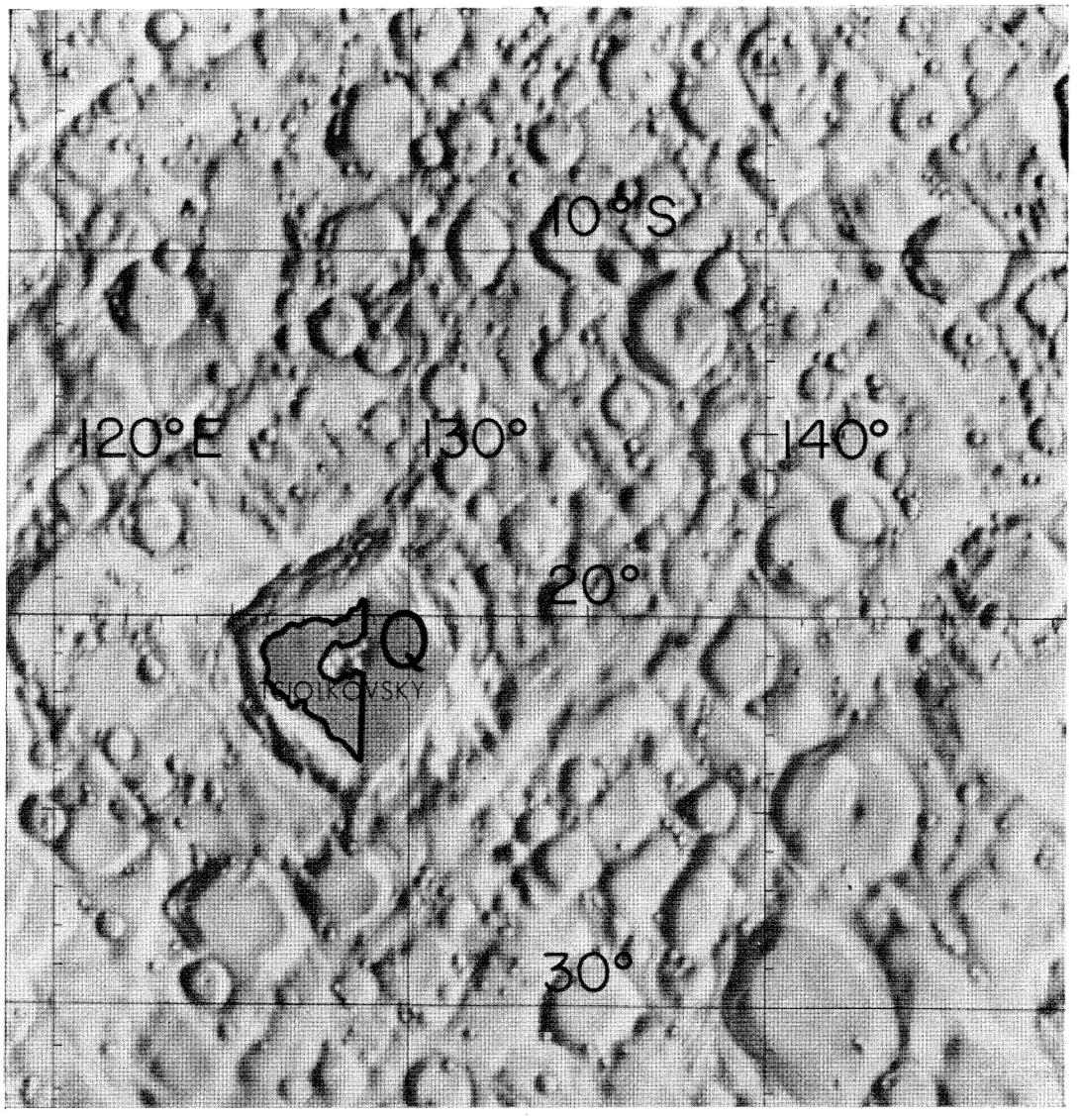

FIGURE 3. Extent of 'area Q' in the large crater Tsiolkovsky (farside of Moon).

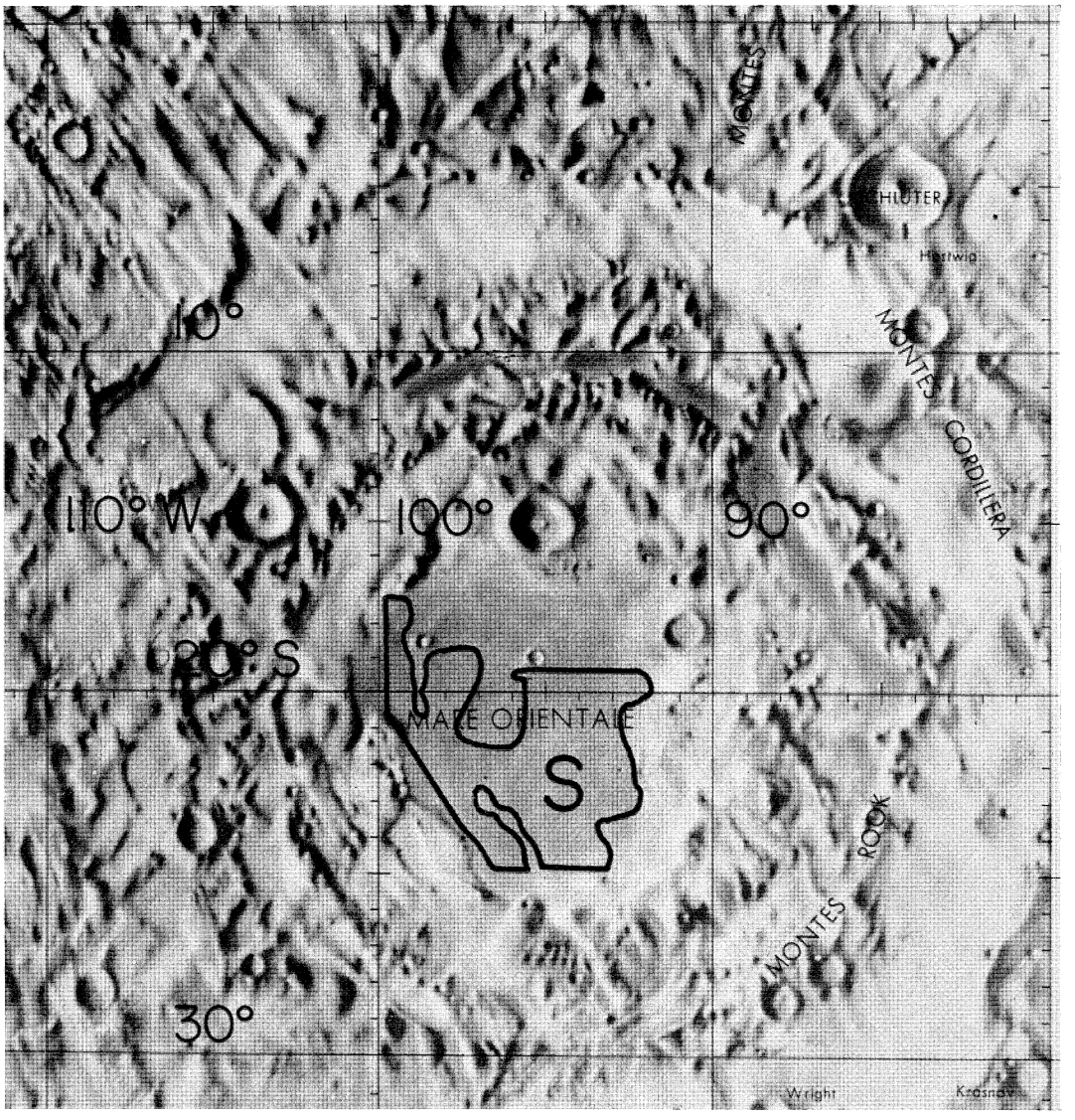

FIGURE 4. Extent of 'area S' in Mare Orientale (limb area).

large number densities of both eumorphic and submorphic craters were encountered and here the data were split subjectively (G.F.) to cover these two types. In all other areas, all types of crater were treated as one. The reason was that morphologic criteria could be misleading. For example, a submorphic crater may be an eroded eumorphic crater or it may be in a class of its own. There may be no monotony of transition from one type to the other.

The problem of the 'true' diameter in a crater is difficult to resolve. At present the best solution is the standardization of the procedure adopted so that a homogeneous set of data is produced. Ideally some absolutely objective method, such as automatic processing, is required but, in the case of the gradational tones encountered on the Moon, automatic measuring must await the development of pattern recognizing devices capable of the complex task required. For this study diameters were measured directly from the photographic print with a graduated straight edge. That the subjective effects so introduced could be satisfactorily minimized is demonstrated in § 2.2.

Areas for study were selected on the basis of the following criteria: (*a*) the areas were to be in the lunabase where number densities were relatively low; (*b*) large craters were to be as far as possible from the areas selected, in order to minimize the number of 'secondary' craters in the study areas and render the obliteration effect negligible; (*c*) the areas were to be large and at widely different locations on the surface of the Moon, in order to attempt comparison studies between the near and far sides of the sphere, between regions at different selenographic latitudes and longitudes, and between different maria; and (*d*) the *Orbiter* prints were to be of the highest quality and taken nearly vertically. With these points in mind, nineteen areas were selected on the near side of the Moon (figure 1), two on the limb (figures 2, 4, plates 5 and 7), and one on the far side (figure 3, plate 6). The areas were given alphabetic designations; their parameters are described in table 2.

Exceptions to criterion (*b*) were made for areas G and H, which include the craters Flamsteed and Arago, respectively, because of the interest surrounding the rings Flamsteed P and Lamont. (Guest & Fielder (1968) consider these to be volcanic ring complexes.) In addition, one exception was made to criterion (*d*): the Mare Crisium photograph had several defects. The area is included since it is the only one located at a selenocentric longitude of around 60°.

Each *Orbiter* print is a mosaic of strips laid side by side. We scanned each strip, or framelet, for craters and measured every crater with a straight edge calibrated in millimetres. In some of the photographs the craters were slightly, but perceptibly, foreshortened and in these cases true diameters were measured. Separate counts were made of craters larger than or equal to 1 mm in diameter in each increment of 1 mm. (In the case of a few areas counts of craters in the $\frac{1}{2}$ to 1 mm increment were also made.) The counts for a given range of size of crater for all the framelets forming one complete area were then totalled.

During this procedure one of two kinds of map was prepared of the area under examination. One kind was such that all craters larger than the truncation size were represented as black disks defining both positions and sizes; the other merely represented the positions of the centres by dots. The first kind of map was used for photometric studies of clustering of craters and will be discussed in § 3.3. Both kinds of map were prepared on clear acetate placed in contact with the U.S.A.F. *Orbiter* prints designated in table 2. The acetate was marked using fine pens. To prevent smudging of the spots, and to facilitate the positional distribution counts, the maps were then copied photographically and enlarged to approximately 45 cm × 58 cm. Unequal shrinkage of the photographic paper was measured by means of a photographed grid. Distortion of up to 1.5% was

found to be present. This source of error was considered negligible and no corrections were applied to our positional measurements.

2.2. *Population curves of lunar craters*

As a requirement of the present programme we examined the frequency distribution of the numbers of craters counted in each test area as a function of crater size. It is general practice to plot cumulative number (that is, number per unit area larger than assigned minimum diameter) as ordinate, against minimum size, as abscissa, and to use logarithmic scales. This practice smooths

TABLE 2. CHARACTERISTICS OF AREAS STUDIED (FOR LOCATIONS, SEE ALSO FIGURES 1 TO 4)

area designation	carto-grapher	Mare	largest named feature in area	area of count/ km²	smallest crater mapped/ m	largest crater mapped/ km	total no. of craters mapped	crater density†	slope $\bar{G}$
A, IV.H-127	I.R. B.W. G.F.	Imbrium	Carlini D	78790	700 350 700	9.4	1029 7989 619	10	3.5
B, IV.H-127	B.W. I.R.	Imbrium	Le Verrier	84327	700 500	21.1	950 2031	11	3.3
C, IV.H-90	I.R. B.W.	Serenitatis	Bessel	32367	643	15.8	685 561	12	3.5
D, IV.H-85	I.R. R.J.F.	Serenitatis	Deseilligny‡	19563	633 317	2.5	415 1042	10	2.8
E, IV.H-90	I.R. B.W.	Serenitatis	Bessel A	32122	643	7.8	554 666	14	4.0
F, IV.H-85	I.R. R.J.F.	Serenitatis	Le Monnier B	19079	634 317	5.1	557 721	8	3.6
G, IV.H-143	G.F.	Procellarum	Flamsteed P	70100	126	20.6	30416	17	2.7
GA, IV.H-143	G.F.	Procellarum	Flamsteed K	3230	156	3.7	919	14	2.8
H, IV.H-85	G.F.	Tranquillitatis	Lamont	36750	100	26.0	1457	8	3.0
J, IV.H-140	R.J.F	Frigoris	Fontenelle G	52054	405	4.5	1460	7	3.0
K, IV.H-54	G.F.	Crisium	Picard Y	47090	670	22.6	699	15	3.9
L, IV.H-143	R.J.F.	Humorum	Doppelmayer K	43213	320	6.0	2637	11	2.7
M, IV.H-137	R.J.F.	Humorum	Gassendi O	17100	335	11.0	808	9	2.7
N, ORB-I-5(100)	U.S.A.F.	Medii	Oppolzer A	2942	426	3.7	836	19	4.8
NA(e), III.M-94	G.F.	Medii	Pallas V‡	2582	116	2.6	3004	23	3·7
NA(s), III.M-94	G.F.	Medii	Pallas V‡	2582	116	1.4	5645	23	3.7
P, I.M-12	C.T.	Smythii	—	16103	360	10.8	681	5	2.4
Q, III.H-121	B.W.	Tsiolkovsky	Tsiolkovsky	5906	380	1.9	941	11	4.3
R, IV.H-91	B.W.	Frigoris	Gartner F	39072	703	14.0	1302	33	3.4
S, IV.H-195	B.W.	Orientale	—	27927	650	17.9	1222	30	4.0
T, I.M-32	B.W.	Foecunditatis	Taruntius G	15366	460	9.9	1558	22	3.4
U, IV.H-113	B.W.	Nubium	Turner	31673	685	11.8	969	28	4.1
W, IV.H-113	B.W.	Nubium	Lassell E	37188	663	4.7	754	15	3.8

† Adopted total number of craters > 700 m diameter per 1000 km² of surface.
‡ Crater outside area.

data fluctuations and, indeed, plots of this type have the mathematical advantage that they are commonly found to be approximately linear. On the other hand, any linearity found without proper attention to the weighting of data may be false, as Chapman & Haefner (1967) showed. In a careful analysis of the data for lunar craters upward of a few kilometres in diameter, listed by Arthur *et al.* (1963, 1964, 1965, 1966), MacDonald (private communication, 1967) showed that, even allowing for incompleteness of observation and deficiencies in counts as the limb of the Moon was approached, there was a curvature in the logarithmic plots of cumulative numbers

of craters against their diameters. Our present results relate largely to a smaller class of crater but, even when the data are represented as log cumulative numbers against log minimum diameters, there is no theoretical justification for a straight line law (Chapman & Haefner 1967). There is thus no justification whatever for extrapolation of the data either beyond the specific diameter range considered, or beyond the boundaries of the area examined.

We agree with Chapman & Haefner's comments that incremental representations of data can be more informative than the cumulative method. Chapman's (1968) later work demonstrates this very well. However, the lunar data used by many authors do not readily qualify for incremental representation. The reasons are that (*a*) observational losses can set in earlier than

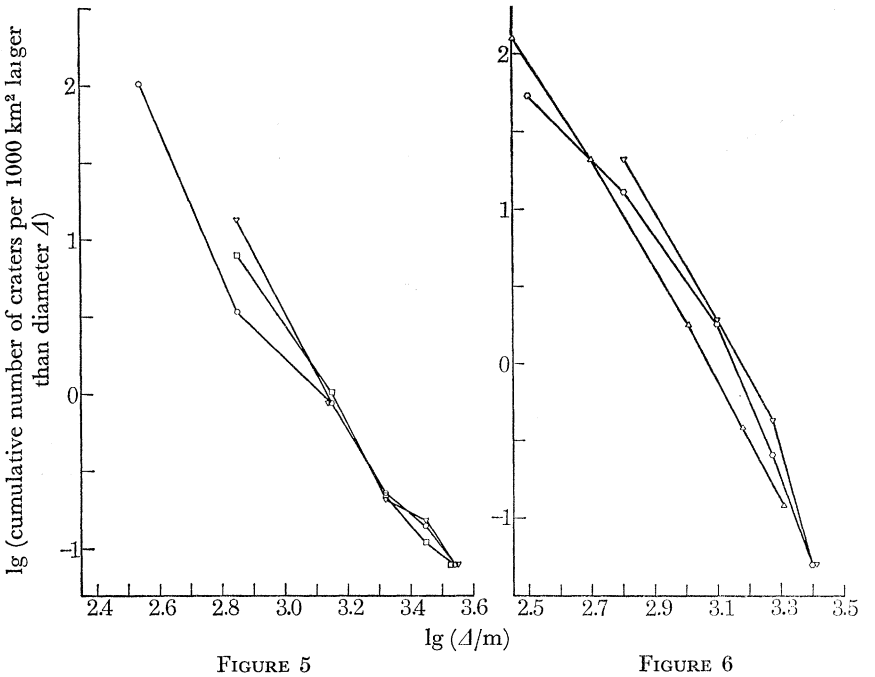

FIGURE 5 FIGURE 6

FIGURE 5. Comparison of population curves by three observers for area A. ▽, I.R.; □, G.F.; ○, B.W.
FIGURE 6. Comparison of population curves by three observers for area D. △, C.T.; ▽, I.R.; ○, R.J.F.

many observers appreciate—especially if all types of crater rather than just eumorphic craters are being counted; losses occur earlier for submorphic craters than for eumorphic craters; completeness of counts depends on the lighting conditions; and losses are not directly proportional to photographic resolution; (*b*) different observers may record widely different numbers of craters on a given photograph, the difference increasing with diminishing crater size; and (*c*) samples are commonly drawn from too small an area. These effects will now be discussed in some detail, on the basis of logarithmic cumulative curves which, of course, tend to mask the differences between different observers.

In order to investigate subjective effects, we arranged that five test areas be counted by more than one individual. The areas will be considered separately.

Area A (figure 1). An inexperienced observer (B.W.) counted 7989 craters larger than 0.5 mm and 266 larger than 1 mm. An experienced observer (G.F.) counted 619 craters larger than 1 mm; and an observer (I.R.) with moderate experience counted 1029 craters larger than 1 mm. All observers used the same photograph, which was of high quality and not the most difficult to

interpret. Counts of the larger craters were in satisfactory agreement. These results are presented in figure 5.

Careful diagnosis revealed that B.W. had included too many craters in the $\frac{1}{2}$ to 1 mm group at the sacrifice of the 1 to 2 mm group, and that I.R. had again included too many craters in his smallest group, 1 to 2 mm. Apparently, aware of the possibility of losses of small craters, B.W. and I.R. had tended to count craters just smaller than the lowest limit. It was found that G.F. had lost some craters in his smallest group. A slope† of modulus 3.5 may be adopted as the best overall slope for area A, although the different observers had given extremes of 3.0 and 3.8.

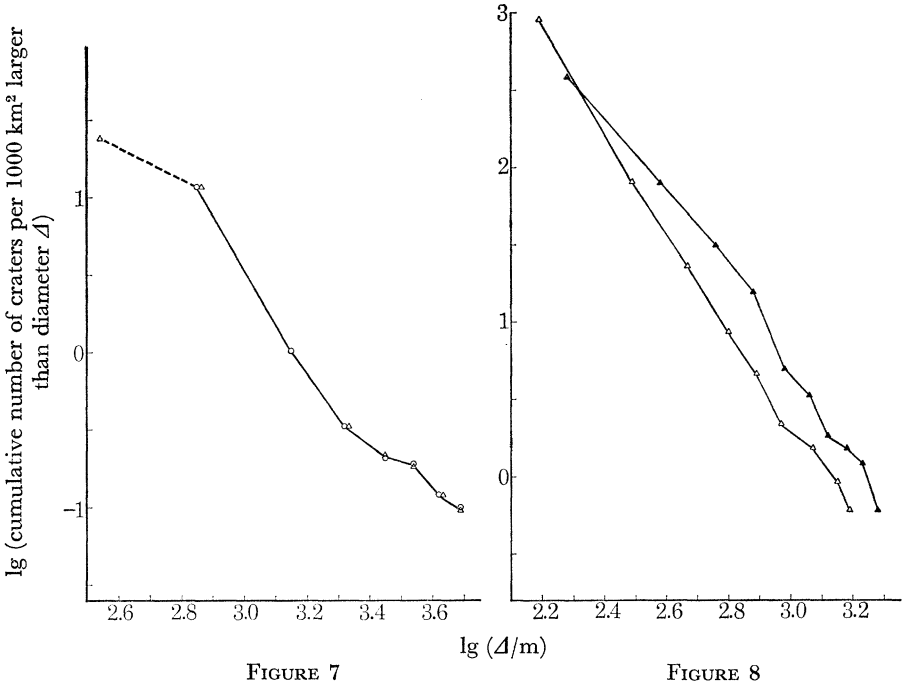

FIGURE 7 FIGURE 8

FIGURE 7. Comparison of population curves by two observers for area B. △, C.T.; ○, B.W.

FIGURE 8. Comparison of population curves for area GA obtained by measurements of a photograph and of an A.C.I.C. map. △, C.T. (A.C.I.C., *Orbiter I*); ▲, C.T. (G.F., *Orbiter IV*).

Area D. Three observers counted the craters in this area and their results are presented in figure 6. The most experienced observer was R.J.F., whilst C.T. and I.R. were both moderately experienced. The agreement between two (R.J.F. and I.R.) is reasonably good except at the smallest diameters where, as in the case of area A, I.R. appears to have included many craters just smaller than his lowest limit. The third observer (C.T.) obtained consistently lower frequencies for the larger craters. Comparison of the original records showed that the discrepancy was due to personal judgement in the inclusion or rejection of submorphic craters, several of which occurred in one part of this area. Most of the areas we selected did not contain as many dubious craters. In spite of this difficulty, the graphs of each observer could be fitted best with a slope of about 3.3.

Area B. Two observers (B.W. and C.T.) were alerted to the pitfalls revealed by the areas A and D results and extremely satisfactory agreement was attained (figure 7). C.T. counted craters smaller than 1 mm and it would appear from the appropriate part of the polygon (broken line

† All slopes are negative. Hereafter, the word 'modulus' will be omitted for brevity.

in figure 7) that he lost craters in this group. Similar losses were suspected in a count by G.F. on area H.

Area S. Two observers (B.W. and G.F.) again attained virtually complete agreement on counts of craters down to 1 mm of photograph of this area.

Area GA. This area was charted by the Aeronautical Chart and Information Center of the U.S.A.F., from an *Orbiter I* photograph, and by one of us from a better quality *Orbiter IV* photograph. Counts on both charts were made by C.T. and are represented in figure 8. The A.C.I.C. data yield a slope of 3.3 and our data give 2.8 for craters of the same range of size. The difference appears to be due to photograph quality, since the data drawn from the poorer photographs are consistently deficient in large craters—presumably submorphic craters.

Counts of smaller craters in the Flamsteed P region (site P-12 of the Lunar Orbiter III Sites Missions) were presented in a Langley Working Paper (1967). Whereas our data and the A.C.I.C. data refer to craters mostly between 170 m and 2 km diameter, the Langley data for craters 200 to 330 m diameter require a slope of 4.5 and, for craters 20 m to 200 m diameter, a slope of 3.7. The areas selected for study are very small and the number of data few, so these high slopes need be of no great concern except to warn of the possible hazards in work of this nature.

The lesson to be drawn from these analyses on five test areas is that (*a*) even when data are presented in the logarithmic cumulative form, rather than in the incremental form, large differences of slope and intercept can be found, in special cases, between different observers and even for the same range of size of crater; (*b*) comparison of slopes of different areas studied by different authors is not necessarily a procedure in which confidence may be placed; (*c*) theories of crater origin based on measurements of the slopes of lunar crater frequency functions and comparison with model functions such as those of Marcus (1964, 1966*a*, *b*, *c*) are not necessarily reliable.

In such an extensive programme as the present one, we have been forced to use counts made by the different observers listed in table 2. For this reason, and for the reasons listed above, we have adopted the logarithmic cumulative form of representing our data rather than the incremental form. The main use to which we put the measured slopes and intercepts is simply in the generation by computer of model crater distributions for comparison with the observed distributions. This procedure will be described in § 3.3. Although, in addition, we make a comparison of the slopes we obtain for different regions and different sizes of crater, we place significance on the difference between slopes only when their ratio exceeds 1.3.

On completion of the analyses of the five test areas by different observers, we proceeded to count the craters in all the remaining areas as carefully as possible. The general form of the plots may be seen in figures 9 to 11.

The most reliable data occur in the middle regions of each plot. At the small diameter end there may be slight losses of numbers. At the large diameter end the number data are few.

We examined the data for areal changes of the parameter, ρ, the number density of craters with diameters greater than 700 m. The adopted values of ρ are listed in table 2. The corresponding values of $\bar{G}$, the modulus of the mean slope in the central portion of each cumulative plot, are also listed.

Variations in ρ are surprising. The mean value of the 22 values of ρ is 15 and the standard deviation from the mean is 7.6. In the case of four areas—NA, R, S and U—the respective densities exceed three times this value. The ratio of the smallest to the highest crater density found in our 22 areas is $33/5 = 6.6$.

There was no obvious general dependence of ρ on selenocentric distance, measured from the centre of lunar coordinates, or on selenocentric longitude λ (figure 12). There may be some dependence of ρ on β, the selenocentric latitude (figure 13). In particular, analysis of those data points that refer to the central meridional region defined by $|\lambda| < 20°$, isolated as solid points in figures 12 and 13, show that there is a tendency for ρ to increase as λ decreases to zero and that there is a strong tendency for ρ to increase as β decreases from 60°. A similar result for bright craters was found by Fielder (1966).

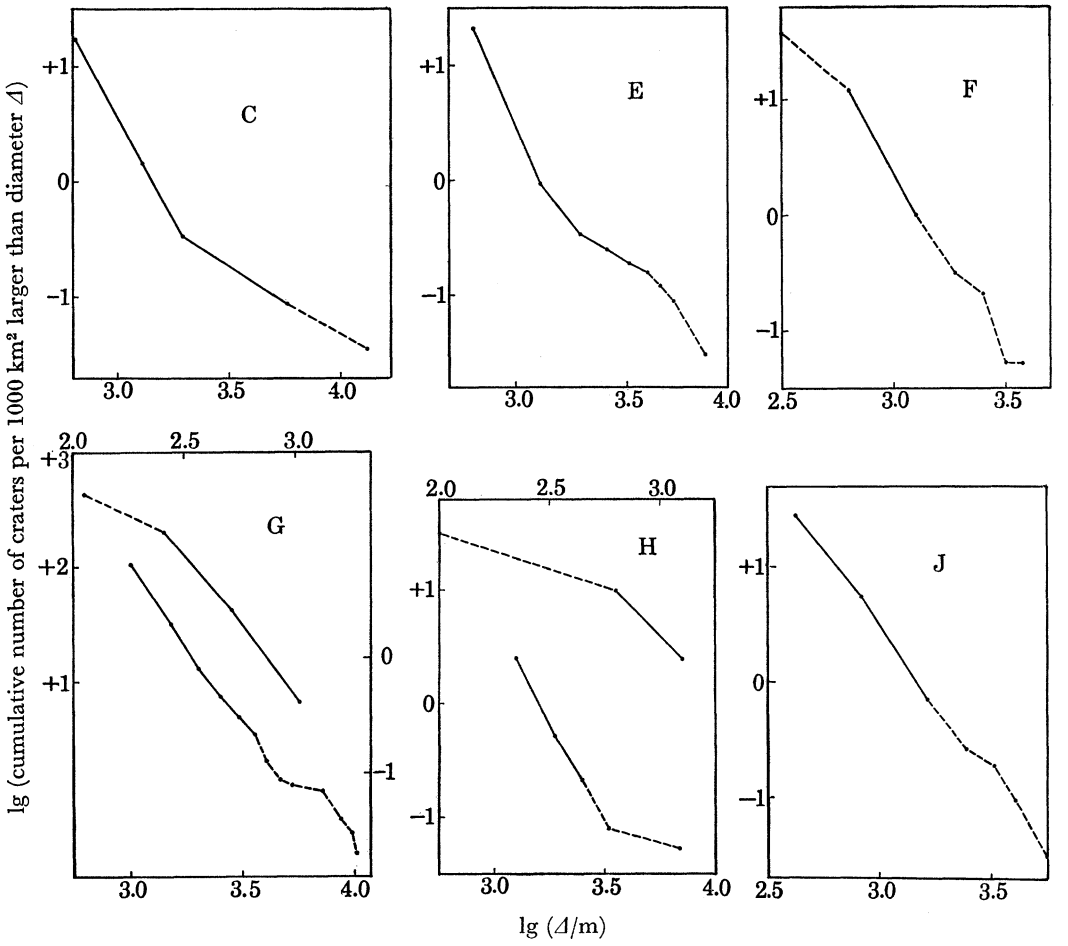

FIGURE 9. Population curves for six areas.

The correlation coefficient for the nine solid points in figure 13 is -0.77; but the data pertain only to the nine areas A, B, C, E, J, N, NA, U and W, and we have not proved that there is a general increase in crater density through all mare regions as the equator is approached along the central meridional strip. Nevertheless, our observations drawn from the central meridional region point to a concentration of craters within 5° of the centre of the lunar disk. One possible explanation is that meteoroids were focused there by the Earth's gravitational field; another explanation is that there was more intense endogenic activity in the central regions of the lunar disk than elsewhere.

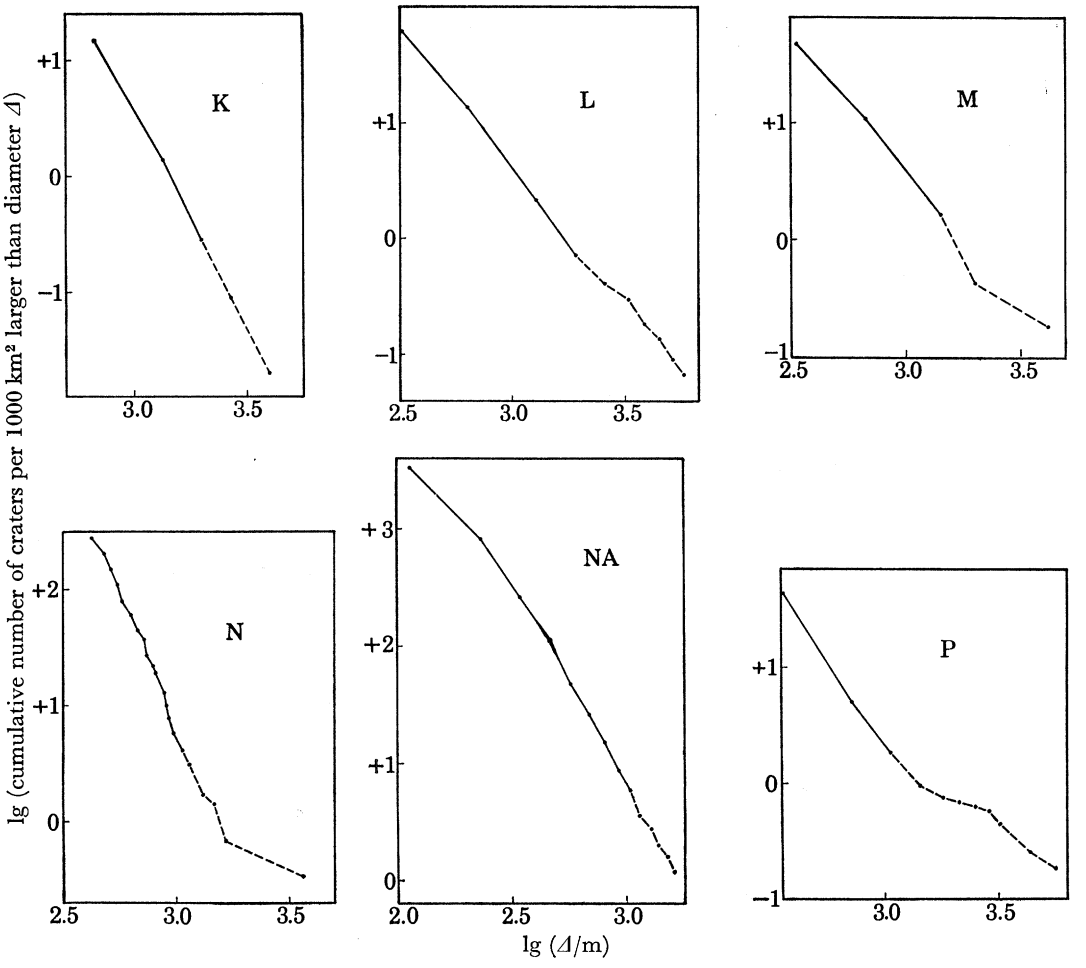

FIGURE 10. Population curves for six areas.

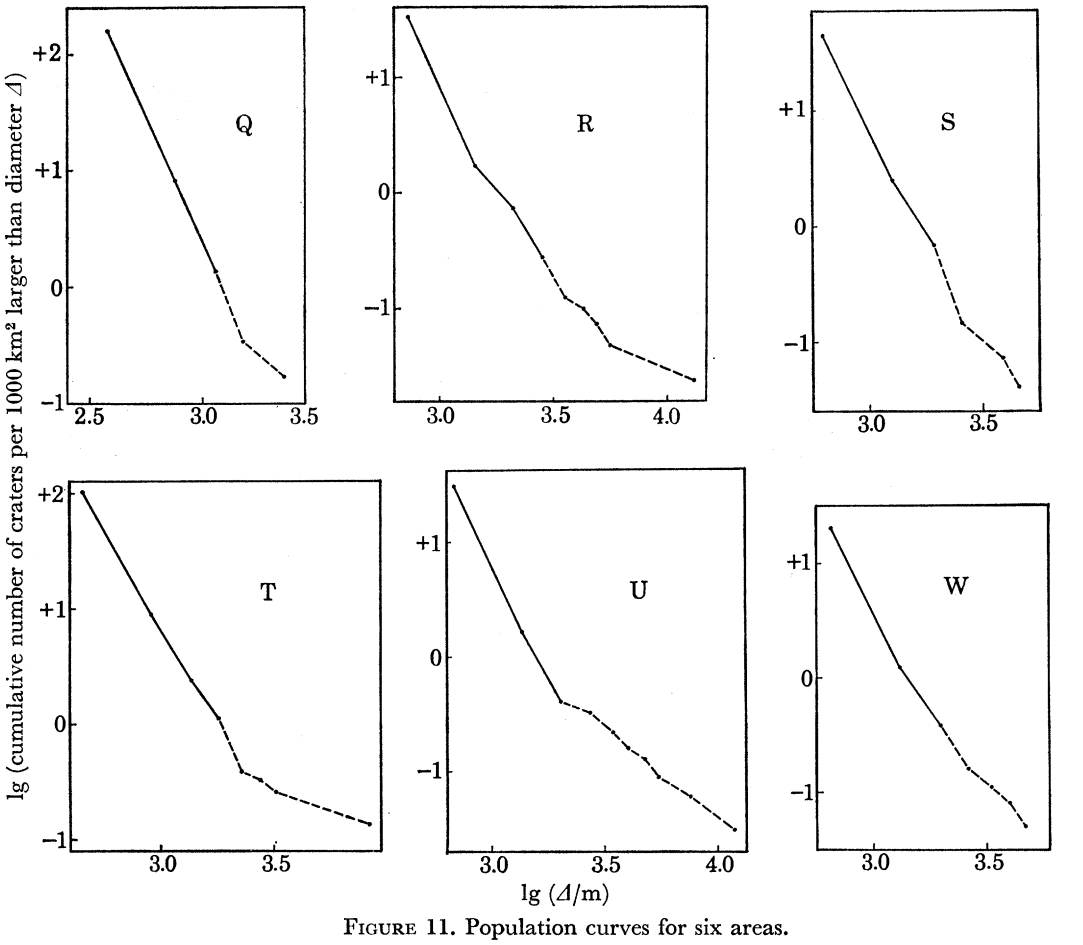

FIGURE 11. Population curves for six areas.

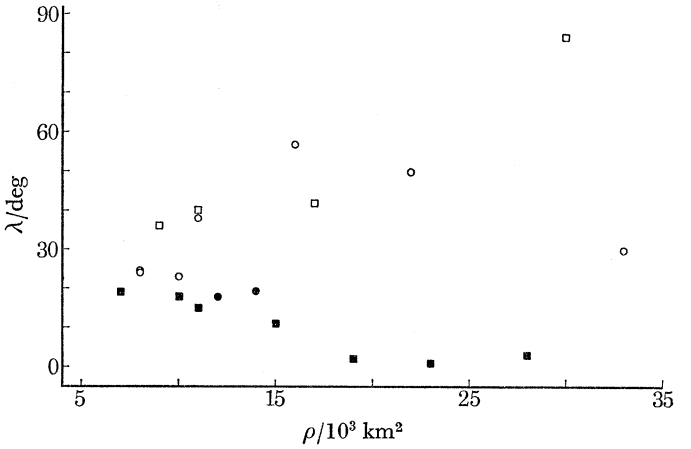

FIGURE 12. Variation of number density, ρ, per 1000 km² for craters $\geqslant$ 700 m in diameter with longitude, λ. Solid symbols refer to areas of $\lambda < 20°$. ○, East longitude; □, west longitude.

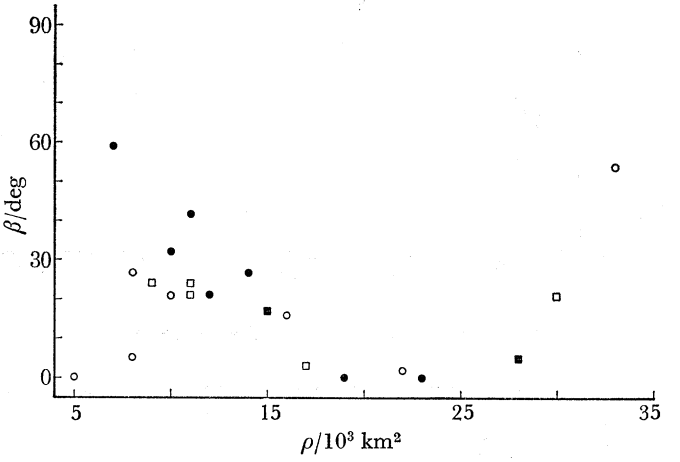

FIGURE 13. Variation of number density, ρ, per 1000 km² for craters $\geqslant$ 700 m in diameter with latitude, β. Solid symbols refer to areas of $\lambda < 20°$ (cf. figure 12). ○, North latitude; □, south latitude.

3. TESTS FOR ALINEMENT AND CLUSTERING OF CRATERS

3.1. *Manual strip tests*

The enlarged print of each of the dot maps corresponding to the areas lettered in table 2 contained a known number of points. Prints were examined, in turn, for the nature of the distribution of points they portrayed. This was done by counting points in a square block of five equal strips, following the statistical sampling procedure described by Fielder & Marcus (1967).

In general terms, the procedure consists of determining the number of crater centres which fall within the boundaries of r equi-areal, parallel strips placed randomly within the area under investigation. The process is repeated for a number of strip azimuths relative to some fixed direction within the area and, for each set of data so obtained, the 'Poisson index of dispersion', V, is calculated from

$$V = S_{N^2}/\bar{N}, \tag{1}$$

where

$$\bar{N} = \sum_{i=1}^{r} N_i/r \tag{2}$$

and $$S_{N^2} = \sum_{i=1}^{r} (N_i - \bar{N})^2/(r-1), \tag{3}$$

$N_1, \ldots, N_r$ being the respective numbers of crater centres observed to fall within each of the r strips.

The test distinguishes between the null hypothesis, H_0, of a stationary, two-dimensional Poisson process and the alternative, H_1, of a stationary, first-order process (a compound Poisson process) in two dimensions. The statistic $(r-1)\,V$ is distributed asymptotically as the product of a constant, C, and a χ^2 random variable with $(r-1)$ degrees of freedom. The constant C is related to the extent of grouping in a given regional array and is given by

$$C = \frac{\text{av}\,(\nu^2)}{\text{av}\,(\nu)},$$

where ν is the number of points per group. For a true Poisson process, each group has just one point and $\nu = 1$, hence $C = 1$. If values of $\nu > 1$ are permitted av $(\nu^2) >$ av (ν) and $C > 1$. Hence H_0 may be rejected in favour of H_1 at level α if the observed value of $(r-1)\,V$ exceeds the $100\,(1-\alpha)$ percentile of χ^2 with $(r-1)$ degrees of freedom.

When $0 < V \ll 1$, equation (3) indicates that, for all values of i, $N_i \approx \bar{N}$, that is, the craters are exceptionally uniformly distributed throughout the area. For instance, we would expect sampled points situated at the intersections of a regular lattice, in which the spacings were small by comparison with the strip width, to give a small value of V.

On the other hand, $V \gg 1$ indicates a degree of clumping of sampled points over and above random fluctuations in number density. Sampling with strips having length l equal to the breadth b (i.e. with squares) would indicate clustering in general, but would be insensitive to a type of clustering such as alinements or 'chaining' of crater centres. If, however, the strip had $l \gg b$, then V would be independent of azimuth for 'circular' clusters but would depend strongly on azimuth for elongated clusters, and especially for linear chains of craters. For an area containing appreciable chaining in one direction, the value of V may be expected to attain a maximum for an azimuth parallel to the chain direction. In principle, the greater l is made by comparison with b the greater the sensitivity to precisely linear chaining and the smaller the sensitivity to circular clustering of dimension smaller than l. Gross changes in the number density p over a large area would still be detected as a general increase in V, independently of the azimuth.

In an attempt to extract information on both chaining and clustering from one and the same test, we used $l = 5b$ throughout this paper. With this requirement, the dimensions of a strip were chosen by applying the formula.

$$b = (A/N)^{\frac{1}{2}}, \tag{4}$$

where A was the area of the region under investigation and N the total number of points within that region. This ensured that we allocated an average of five points per strip—a compromise to ensure sensitivity and reliability of the tests.

Throughout the investigations we used sets of 50 sample strips, each set separated by 10° in azimuth so that results for different regions could be compared directly. In particular, we placed the centre of our block of five strips in ten random positions, in turn. Starting with the strip length parallel to an approximately north-bearing line marked on each chart, we counted the number of points in each strip and then rotated the block through 10°, 20°, ..., 170°, respectively, about its centre, counting the number of points in each strip for each rotation position. By this procedure we tended to retain fairly systematic changes in V as a function of azimuth and to

smooth out fluctuations in V due primarily to different fractional inclusion of clusters in a block for different positions of its centre. Use of the procedure also eliminated any edge-of-field effects. Values of V were computed from these observations.

3.2. *Strip tests on control maps*

The foregoing manual tests make it possible to detect chaining and clustering of crater centres but they do not reveal the actual proportions of craters in chains or in clusters. By performing corresponding tests by computer, on known distributions, we were able to estimate the proportion of craters in chains and in clusters, for each field of craters examined.

The computer program consisted, in effect, of performing the test, as described above, on a random two-dimensional array of points held as pairs of numbers in the memory of a C.D.C. 6400 computer. However, since clusters of craters were absent from these arrays of points, block centres were positioned randomly for each azimuth. The arrays of points which may, for all intents and purposes, be regarded as real consisted of a known, constant number of points in a plane, square area of unit size, a known fraction of the points being randomly distributed over the whole area and the remaining fraction, P, being alined parallel to a preassigned azimuth.

The actual distribution of volcanic craters along fractures is complex although, in the terrestial case, it has been claimed (Bullard 1962) that they are regularly spaced, the separations possibly being related to the depth of the crust at that point. It was necessary to specify some model for the simulation of chains, so we distributed the points with constant separation to form chains. Since the actual number density of craters in a sampled area varied from place to place, it was necessary to define some parameter which would relate the separation of the craters along a chain to the number density rather than to the size of the area. However, the value of b defined by equation (4) is dependent only on the number density. This value was, therefore, adopted as the unit of separation along a chain; and hence the separation index, S, of two adjacent craters in a chain was defined by

$$S = s(N/A)^{\frac{1}{2}}, \tag{5}$$

with s equal to the actual separation along the chain.

The artificial distributions thus created were utilized in the following manner. A predetermined number, N, of points was distributed uniformly† over unit area. Care was taken to ensure that the distribution was indeed random, preliminary tests showing the need to modify the standard random number generator for this purpose. The V-test was then performed upon this array and the results (V, P) printed out. Next, the first n points generated by the computer were rearranged (all the points were held sequentially in the computer memory in the order of their creation) in order to introduce an alinement of points with constant separation, s, crossing the entire field parallel to the x-axis. In this way N was held constant. The number, n, of points so rearranged is obtained from

$$n = [(1 - x_1)/s] + 1 \quad (0 \leqslant x_1 \leqslant s), \tag{6}$$

where x_1 is the 'x coordinate' of the first member of the chain. Because of the positional independence of the points, the random nature of the background was not impaired by this procedure.

The coordinate x_1 was chosen in such a way that it had a uniform probability of appearing in the range $0 \leqslant x_1 \leqslant s$. The common '$y$ coordinate' of the chain elements was similarly arranged to have uniform probability within the range $0 \leqslant y \leqslant 1$. Repetition of the V-test gave a result

† In this context, the term 'uniform' means that each point is positioned entirely independently of every other point in the x–y plane, and that each position in the plane has an equal probability of containing a point.

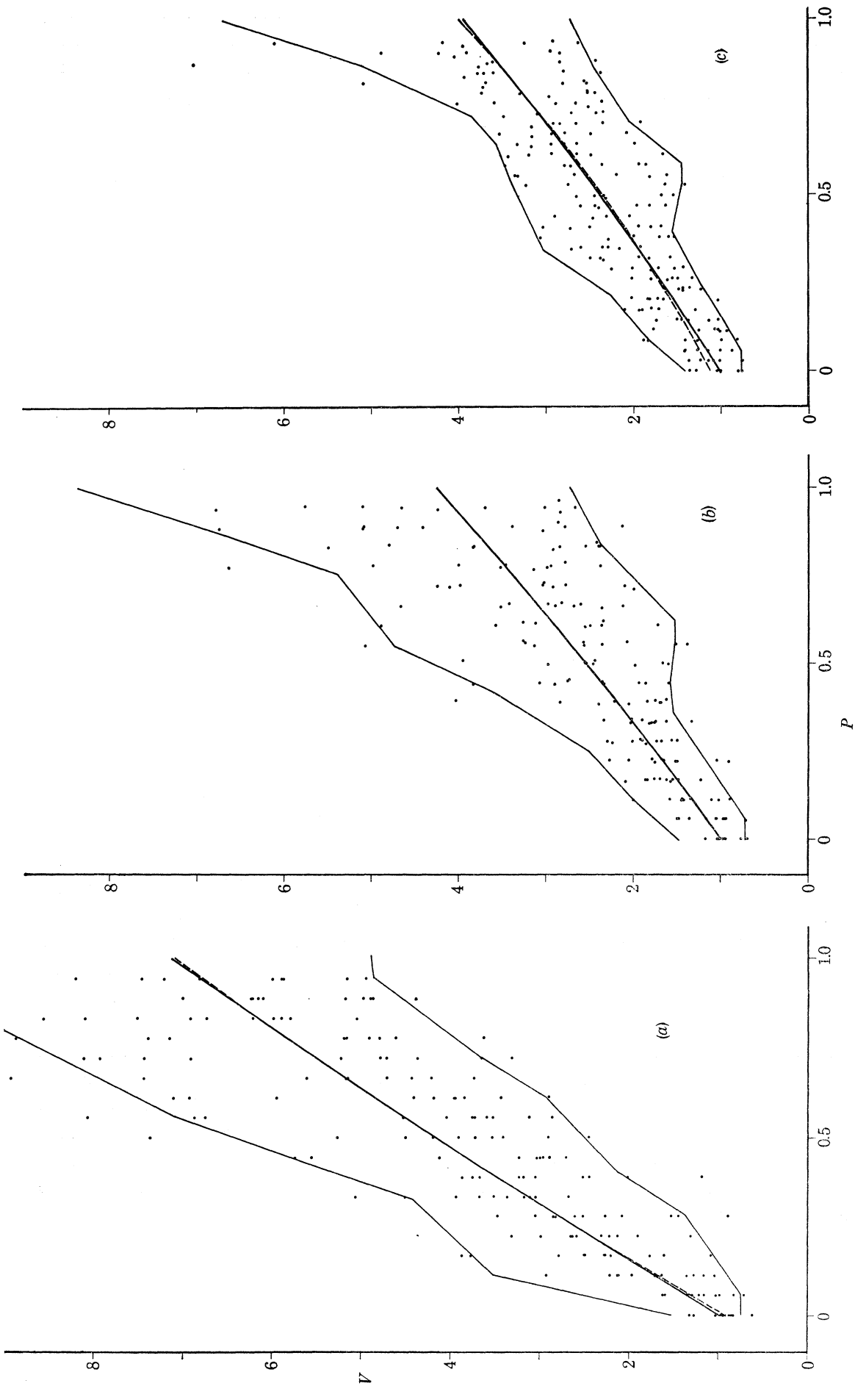

FIGURE 14. Scatter diagrams of index of dispersion, V, against proportion, P, of craters in chains, for three values of separation index, S. (*a*) $S = 0.6$, (*b*) $S = 1.0$, (*c*) $S = 1.4$. The adopted least squares quadratic fit is shown in each case by a heavy solid line, the unweighted (see text) fit being shown, where it differs, by a light dashed line. The light solid lines indicate the 10 and 90% confidence limits obtained as described in the text.

for a distribution with a known proportion, $P = n/N$, of chained points. Additional chains having the same separation were then inserted, the test being repeated after the insertion of each one until all, or nearly all, the points were members of parallel chains. A total of eleven separation indices, S, was used. For each value of S a sufficient number of calculations was performed to give approximately 200 data points in the (V, P) scatter diagram. Examples of the scatter diagrams so obtained are shown in figure 14.

We wished to obtain a family of curves from which, knowing a measured value of V and an estimated value of S, it would be possible to make an estimate of P. To achieve this, quadratics

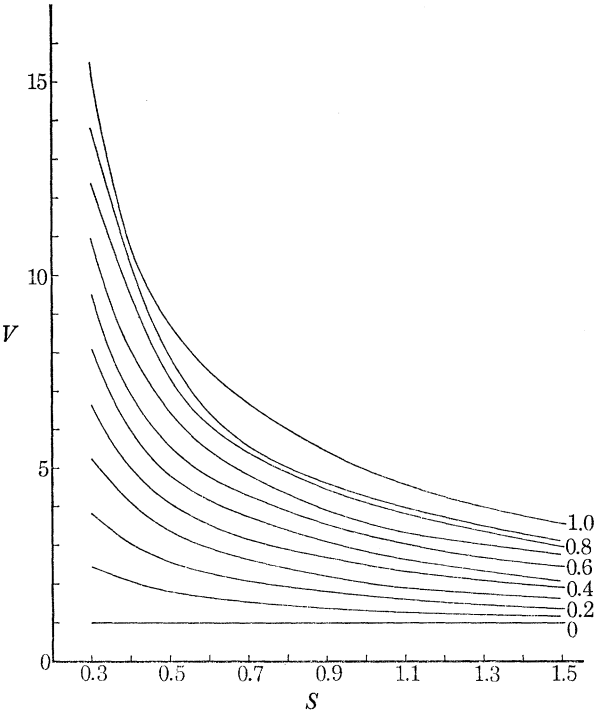

FIGURE 15. Family of curves showing the index of dispersion V against separation index S, for various values of proportions, P, of craters in chains, obtained from the computer simulations. P increases upwards in steps of 0.1 from 0.0 to 1.0.

were fitted by the least squares method to each set of data relating V and P. One quadratic was fitted to the raw data whilst the second was forced to pass through the point $V = 1$, $P = 0$. In each case the difference between the two curves was small (see, for instance, figure 14*c*) but the second curve was considered to be more acceptable in view of the known properties of V. The second curve was therefore taken as an estimate of the 'true' relation between V and P.

An estimate of the scatter of data points around the (V, P) curve was made, in a manner independent of the curve itself, in the following way. Given m data points distributed in an unknown fashion but in one dimension it may be assumed that the lowest point is an estimate of the $p = 100/(m+1)$ percentile of the distribution, the next is an estimate of the $2p$ percentile and so on, up to the highest, which is an estimate of the $(100-p)$ percentile. This arises from the assumed infinitely extended nature of the distribution function and the fact that the density of points is a consequence of the form of the function. The accuracy of the estimates so made increases with m.

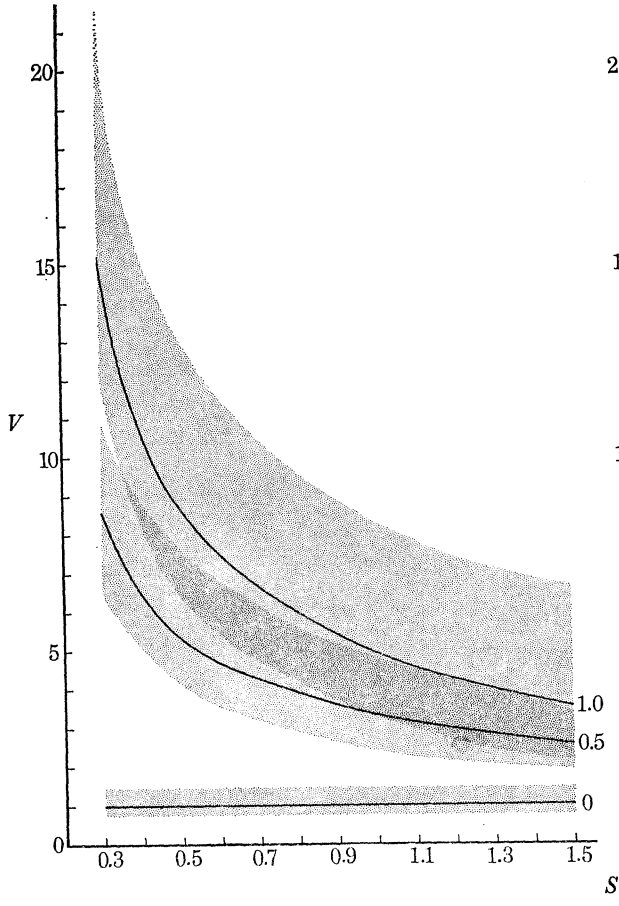

FIGURE 16. 10 % and 90 % limits on scatter in V for three of the curves given in figure 15 corresponding to $P = 0.0$, 0.5 and 1.0.

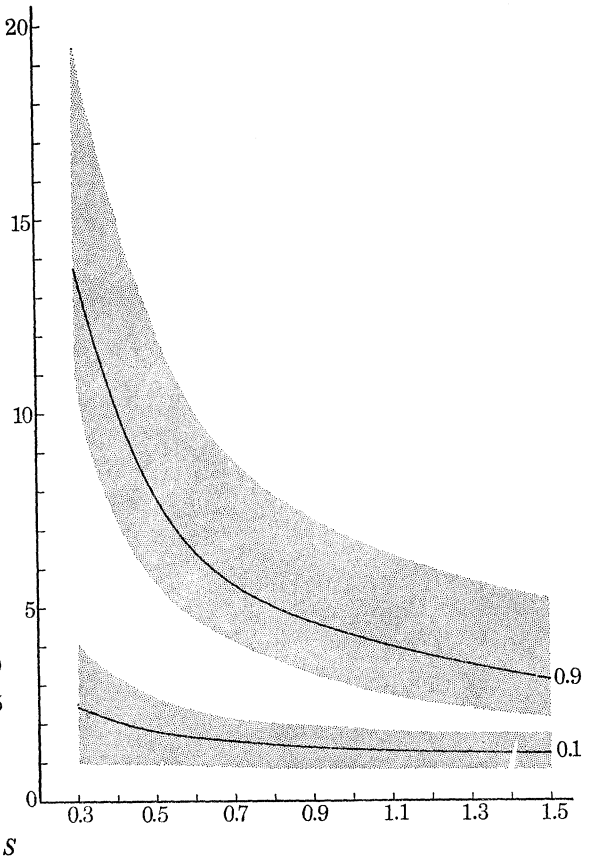

FIGURE 17. 10 % and 90 % limits on scatter in V for two of the curves given in figure 15 corresponding to $P = 0.1$ and 0.9.

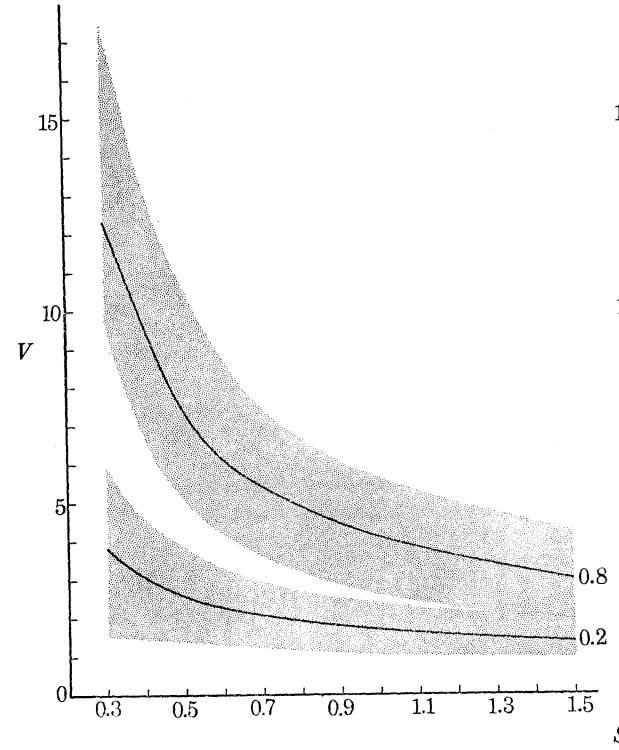

FIGURE 18. 10 % and 90 % limits on scatter in V for two of the curves given in figure 15 corresponding to $P = 0.2$ and 0.8.

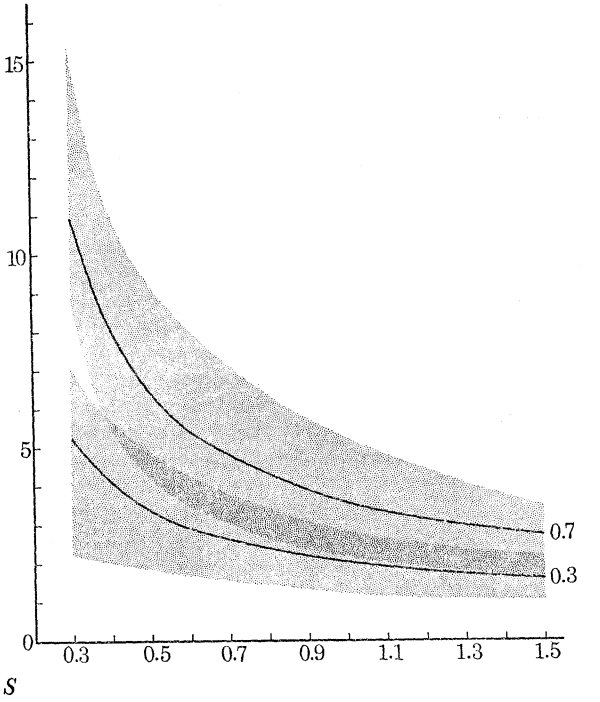

FIGURE 19. 10 % and 90 % limits on scatter in V for two of the curves given in figure 15 corresponding to $P = 0.3$ and 0.7.

Thus the 10th and 90th percentiles of columns of V-values were estimated for particular values of P in the scatter diagrams. In every case at least fifteen values of V were used in these estimations. Adjacent columns were combined if the number per column fell below fifteen: for such combined columns the spread in the values of P did not exceed 0.07. In general, the 10th and 90th percentiles were obtained by linear interpolation between the percentiles estimated from adjacent points in the column. Scatter limits so obtained are illustrated in figure 14.

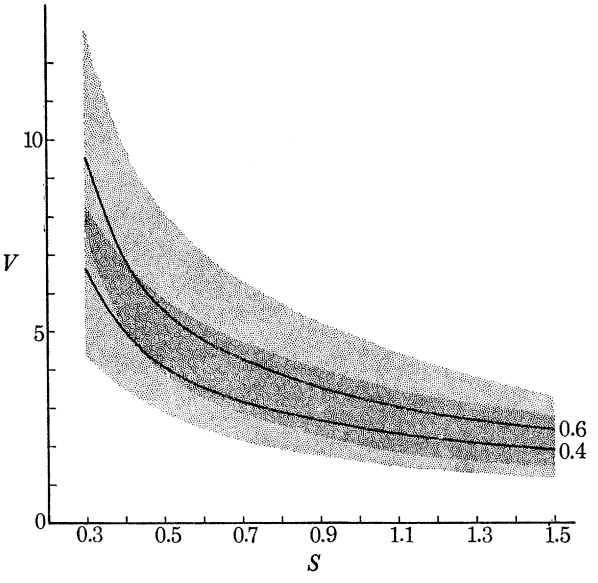

FIGURE 20. 10 % and 90 % limits on scatter in V for two of the curves given in figure 15 corresponding to $P = 0.4$ and 0.6.

Finally, these data were used to build the family of curves of V against S shown in figure 15. The curves are given for constant P in intervals of 0.1 from 0.0 to 1.0 and, because of their close spacing, we have presented the curves separately, in figures 16 to 20, each curve with information on the possible spread in V. The possible limits of P were deduced from these curves.

3.3. *A photometric method to register clustering*

We have already shown (§ 3.1) that a particular value of the index of dispersion, V, contains information on both clustering and alinement of crater centres. We shall attempt to separate cluster craters from chain craters statistically in § 3.5 but, at this point, it will be instructive to consider the problem of clustering in more concrete terms. In this section we demonstrate that, for three sample areas, clustering of the craters we have mapped occurs to a marked extent.

Clustering may be studied in two ways: in considering elemental areas, one may measure the number density of points representing the centres of craters in the xy plane or one may measure the area of surface covered by craters. The total fractional area covered by the craters may be regarded as an indication of the energy (volcanic or impact) released in the region in question. The second method, and the results drawn from it, will be presented first.

Areas B, G and H (table 2) were selected for this investigation because of the possibility of volcanism (Guest & Fielder 1968) in areas G (figure 1) and H and because area B, unlike the other two, is in that part of an 'open' mare in which wrinkle ridges occupy a very small fraction of the field.

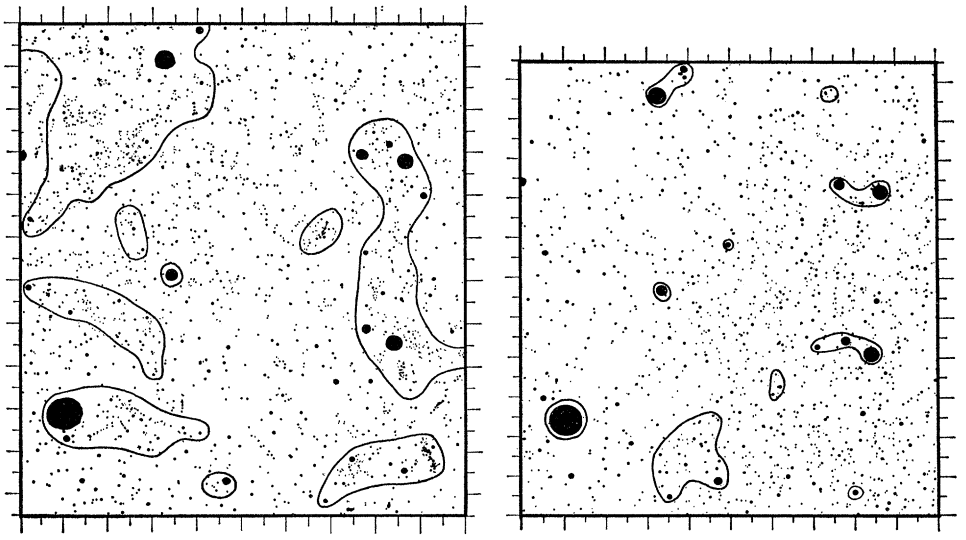

FIGURE 21. Comparison of photometrically derived clustering for area B (true distribution left, quasi-random computer simulation right). Contours corresponding to twice the mean photometric density are shown.

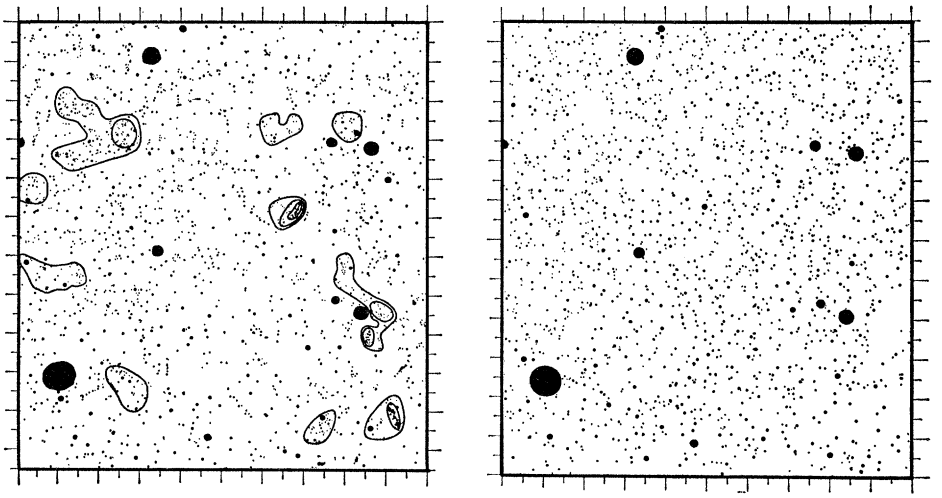

FIGURE 22. Comparison of clustering derived from square counting for area B (true distribution left, quasi-random computer simulation right). Contours correspond to two, three and four times the mean number density. The random simulation shows no clusters of this degree of prominence.

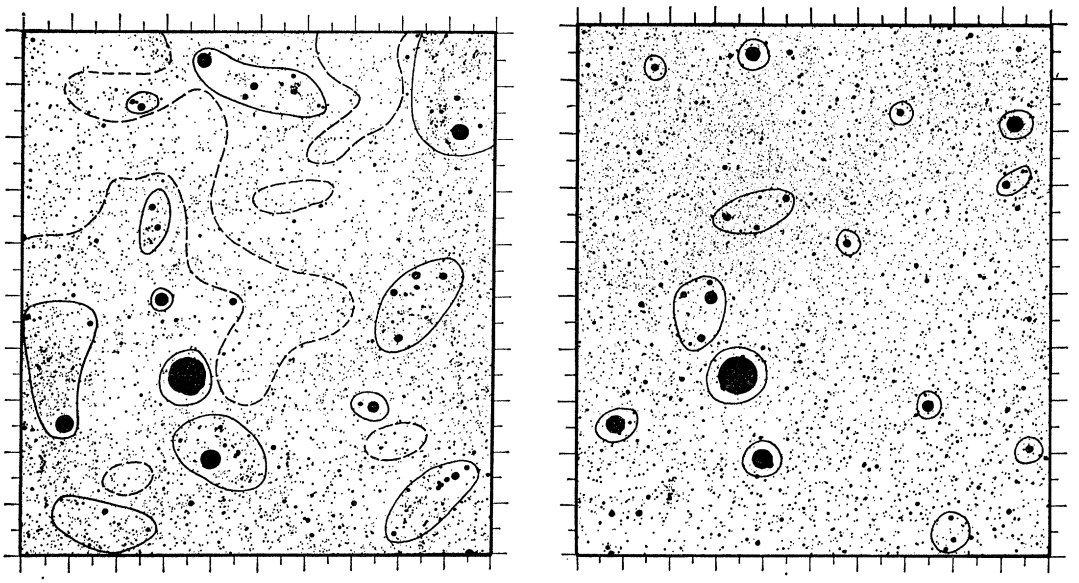

FIGURE 23. Comparison of photometrically derived clustering for area G (true distribution left, quasi-random computer simulation right). Solid contours correspond to twice the mean photometric density, dashed contours to half the mean.

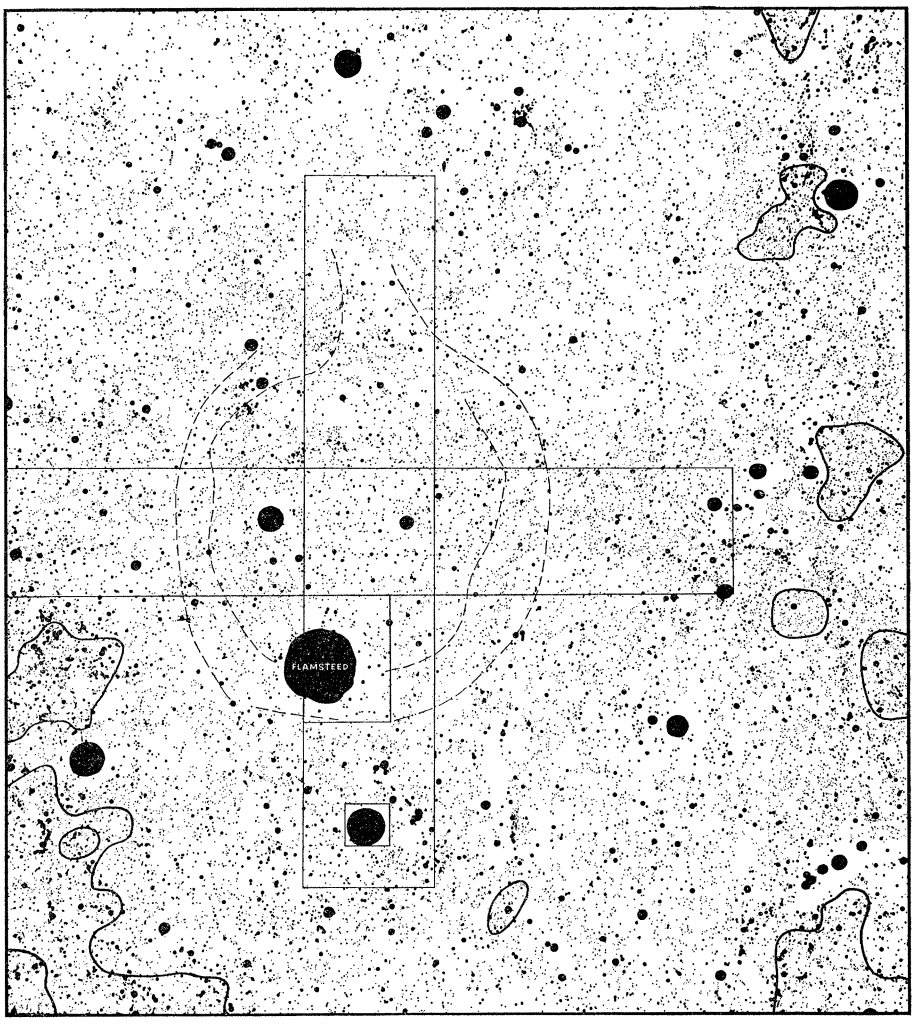

FIGURE 24. Clustering in area G derived from square counting. The solid contours correspond to twice the mean number density, the dashed lines give the position of the walls of Flamsteed P, while the rectangular outlines show the limits of the counted areas for the derivation of figure 31.

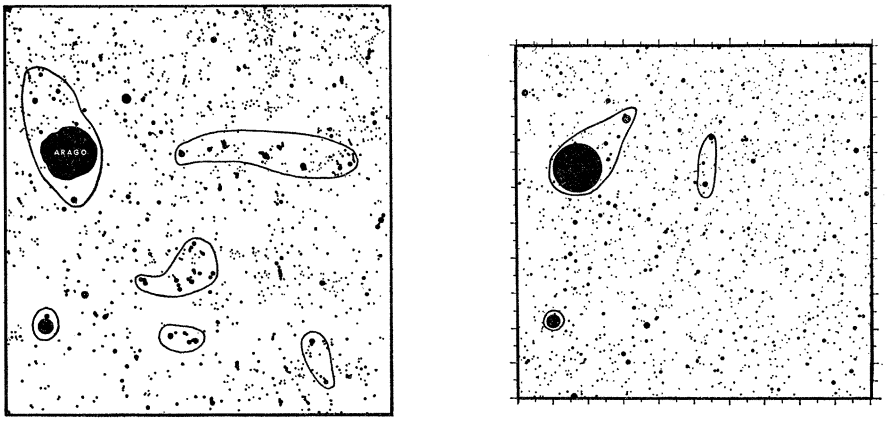

FIGURE 25. Comparison of photometrically derived clustering for area H (true distribution left, quasi-random computer simulation right). Contours corresponding to twice the mean photometric density are shown.

Outlines of all the craters larger than 1 mm of photographic print in each of the three sample areas were prepared and blacked in. The charts so prepared were reduced photographically and recorded on glass negatives. The negatives were then scanned using the Jarrell–Ash Photometer

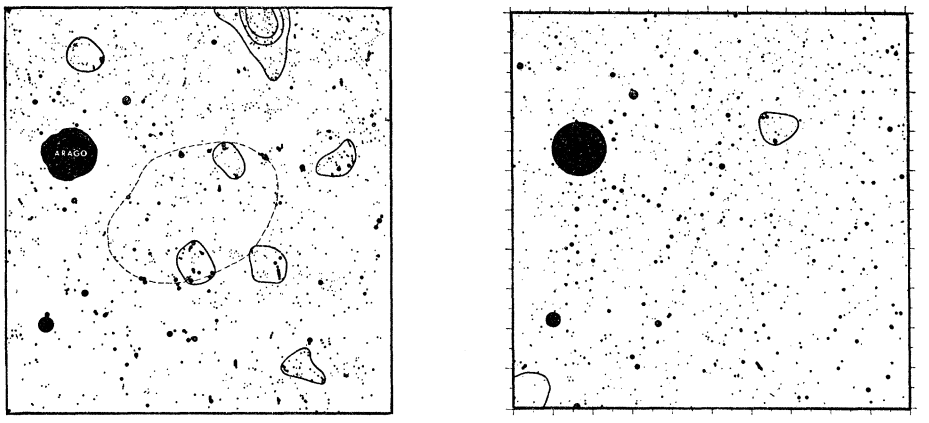

FIGURE 26. Clustering in area H derived from square counts (true distribution left, quasi-random computer simulation right). Solid contours show twice, and higher multiples of, the mean crater density. The dashed line illustrates the boundary of the low ring Lamont.

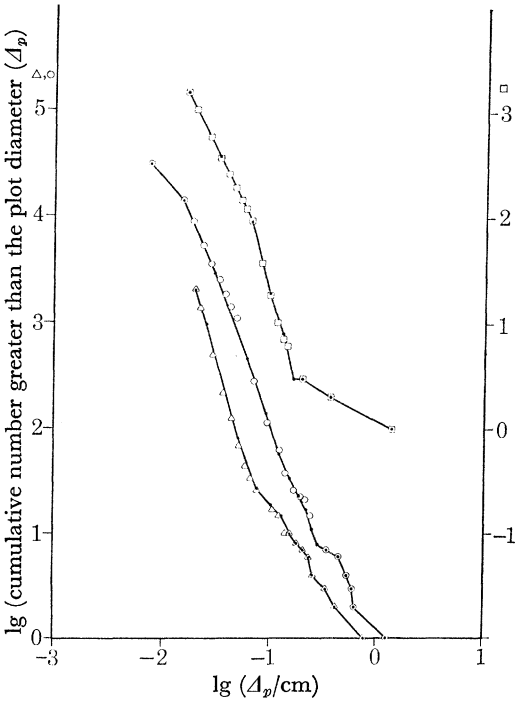

FIGURE 27. Comparison of population curves for the simulated and original test areas. The solid curves correspond to the original areas, the open symbols to the simulations. △, Area B; ○, Area G; □, Area H.

and penrecorder of the Steward Observatory. Since the maps used consisted of black areas, corresponding to the craters, on a white background (figures 21, 23 and 25) the light transmitted by a given region of a negative was proportional only to the areas of the craters in that region.

Although the deflexion of the recording pen accurately recorded the light transmitted by that section of the negative imaged on the slit of the photometer a difficulty arose from the fact that

a single large crater gave the same effect as a cluster of small craters. The effects of this ambiguity on the records were investigated through the simulation of 'control maps' having the same total number density of craters and the same diameter distribution as the maps of the real sample areas, but with the centres of craters in random positions in the xy plane.

The simulations were performed by means of an I.B.M. 1130 computer equipped with a Calcomp 1602 pen plotter. Craters were assigned random positions using the modified random number generator utilized for the strip test simulations. In addition, it was necessary to generate a diameter distribution equivalent to the original in each test area, using uniformly distributed random numbers (see preceding section). Uniformly distributed random numbers were converted to random diameters of the desired form by use of the equation

$$y_i = \Delta / x_i^{1/G}, \tag{7}$$

where y_i was the random diameter required, Δ the minimum diameter permitted, x_i the random number delivered by the computer, and G the modulus of the gradient of the cumulative frequency curve.

This may be readily proven. Given x_i uniformly distributed in the range $0 \leqslant x_i \leqslant 1$, let

$$y_i = b / x_i^c, \tag{8}$$

where b and c are constants. Then $y_i \geqslant b$, and $y_i \geqslant$ some value Y if

$$x_i \leqslant (b/Y)^{1/c}. \tag{9}$$

But this has probability $(b/Y)^{1/c}$ from the distribution of x_i; i.e. the cumulative distribution for the y_i generated from equation (8) must have the form

$$N = B / Y^{1/c}, \tag{10}$$

where B is a constant and N the cumulative number larger than diameter Y. Equation (7) now follows by direct comparison of equation (10) with equation (8).

The required distributions were created in the following manner. Examination of the $\lg N$, $\lg \Delta$ curves of the regions B, G and H, illustrated in figures 7 and 9 shows that they are very 'noisy' at the large-diameter end. The largest ten or so craters in each area were therefore removed from the distributions and the remainder simulated. Even the remaining portions of the curves were not straight, in general, as required for the above theory, so they were approximated by two or three straight-line segments within established diameter limits. The gradients and Δ-limits of each section were then used to generate the N, Δ data appropriate to that section† and the data for all sections pertaining to a given area were combined to form the control map for that area. Finally, the largest craters that had been removed previously were reintroduced into the control simulations at points corresponding to those in the original areas. This procedure simplified the interpretation of the isophote maps: a random redistribution of these few largest craters would have had no value in this case. Comparison of the size distributions of the simulated maps with those of the originals is made in figure 27 and it is seen that the curves approach one another to a satisfactory extent.

Two points are worth noting in this context, however. First, the simulated data shown in figure 27 form the 'nominal' distribution only; that is, the distribution of the data generated by the computer. In fact obliteration of craters as a result of the overlapping of larger ones in the

† Diameters which were found to be too large were rejected.

simulated maps means that a small proportion of the smallest craters have been removed. However, a test showed that, even in the case of the area of highest number density, less than 1.5 % of the total number of craters was lost through obliteration. The effect may therefore be disregarded. Secondly, the diameters indicated are, again, the generated diameters. Small errors in plotting superimpose 'noise' on the programmed diameters, though the effect is no larger, overall, than that of the 'noise' in the original measurements of diameters. However, the pen used to represent the smallest craters of the area *G* simulation was slightly too large, giving this area the appearance of being too dense (figure 23). Similarly, the pen used to plot the smallest craters of area *H* was too small, giving the opposite effect (figure 25). In each case, only the smallest, and most numerous, craters were affected. We found that the photometer was insensitive to these differences and so, again, we were able to neglect them in the final discussion.

Each of the six areas—three originals and three simulations—where scanned photometrically in strips 2.5 mm wide, the size of each negative being such that ten scans covered the entire area. Recording speeds of either 15 or 25 mm/min were used. Repetition of the process at 90° to the original scan direction provided increased accuracy in the results. The observed pen deflexions were integrated to give the total light transmitted by each 2.5 mm × 2.5 mm square of the negative. In this way at least 100 independent intensity measurements were obtained for each area. Examination of the original pen recordings enabled us to remove the effect of the large craters present in both original area and simulation; and the mean intensity of the remaining light transmission was then readily calculated.

The presence of clustering may be demonstrated in two ways. The 'standard error', ξ, in the measured intensities, a, was calculated for each area as a percentage of the mean intensity $\bar{a}$ using

$$\xi = \frac{100}{n\bar{a}}[\Sigma(a \sim \bar{a})^2]^{\frac{1}{2}}, \tag{11}$$

in which n is the number of samples. The results obtained for each area are summarized in table 3.

TABLE 3

area	n	ξ_0 (original)	ξ_s (simulation)	η
B	110	7.0	4.9	1.43
G	100	2.5	1.2	2.08
H	100	7.3	4.8	1.52

The last column of the table gives a numerical measure of the clustering of craters in each area. Through the use of this 'degree of clustering' parameter, $\eta = \xi$ (original)/ξ (simulation), it is possible to compare areas having different mean number densities of craters. In each case, the value of η is appreciably larger than unity, indicating a marked degree of clustering over and above that expected for a model generated by primary impacts.

An alternative, and possibly more convincing, demonstration of clustering is provided by the examination of approximate isophotes superimposed on the crater maps. In this way one may study the distribution of clusters of craters relative to other craters in a field. Contours representing twice the mean light intensity recorded by the photometer are shown for the three maps studied, and for the corresponding control maps in figures 21, 23 and 25. The contour appropriate to half the mean intensity is shown for the area *G* in figure 23.

In all cases the contours are most strongly influenced by the large and medium-sized craters,

and less so by the background of small craters. In the case of area G (figure 23) the contours are closely related to the low walls of the 'ghost' ring Flamsteed *P*. Of necessity the contours are approximate, and are quite insensitive to small-scale crater alinements. This is amply demonstrated in the case of area H (figure 25) where, commonly, the clusters may be seen to be formed of medium-sized craters alined in directions which differ from the long axis of a cluster. Clearly, this technique is of value in distinguishing areas of high volcanic activity or intense secondary cratering.

3.4. *Square counts*

Measurements of clustering by determining the number-density of craters in equal elemental areas may be made using the Poisson–χ^2 method, first applied to the Moon by Arthur (1954). It is usual to calculate a grid of elemental squares such that, on average, each square contains $\bar{z}$ crater centres and then to compare the areal distribution of centres with the corresponding Poisson distribution by means of a χ^2 test. The method is a particular case of the strip-counting method but, unlike the latter, is insensitive to alinements of craters.

To ensure reliability of the test, $\bar{z} \gg 1$ (A. Marcus, private communication). The three areas B, H and G, selected for study, were subdivided into a convenient number of sample areas having $\bar{z} \approx 10$, 11 and 60, respectively. The results drawn from the Poisson–χ^2 method applied to these areas could be compared with those drawn from the photometric method applied to the same three areas. It is important to note that the two techniques are complementary rather than alternatives.

The observed distribution of points (crater centres) in each of the areas selected was compared with the corresponding distribution that had been simulated by the IBM 1130 computer (§ 3.3) and with the corresponding Poisson distribution computed from

$$(f_i)_c = \frac{k}{i!} e^{-z}(z)^i, \tag{12}$$

where $(f_i)_c$ was the number of elemental areas, or cells, expected to contain i craters if they were distributed at random and k the total number of cells. Cells completely or partially covered by the largest crater in each field were not considered in this analysis, because of their known tendency to introduce a departure from randomness. Plots of i against $(f_i)_o$, the number of cells observed to contain i craters, are given for the actual and simulated distributions corresponding to each of the three test areas in figure 28 (area B), figure 29 (area H) and figure 30 (area G) and, in addition, the symmetrical curve in each figure is a plot of i against $(f_i)_c$.

As expected, the points representing the simulated crater field scatter around the Poisson curve in each case. This confirms that the simulated fields of craters conform to a quasi-random† distribution. The departure from the Poisson curve of the polygon of points representing the data drawn from (*a*) the simulations and (*b*) the actual areas on the Moon may be measured by applying the χ^2 test in which (with the usual notation)

$$\chi^2 = \sum_{i=0}^{\infty} \frac{(o-c)^2}{c}. \tag{13}$$

The results are given in table 4, in which ν is the number of degrees of freedom. Tables of χ^2 show that the probability that the simulated distribution matches the Poisson distribution is reasonably high, in each case; but that the probability that the actual distribution matches the corresponding Poisson distribution is, in each case, completely negligible: the observed distributions depart

† As explained in § 3.3, some of the largest craters were placed in special positions.

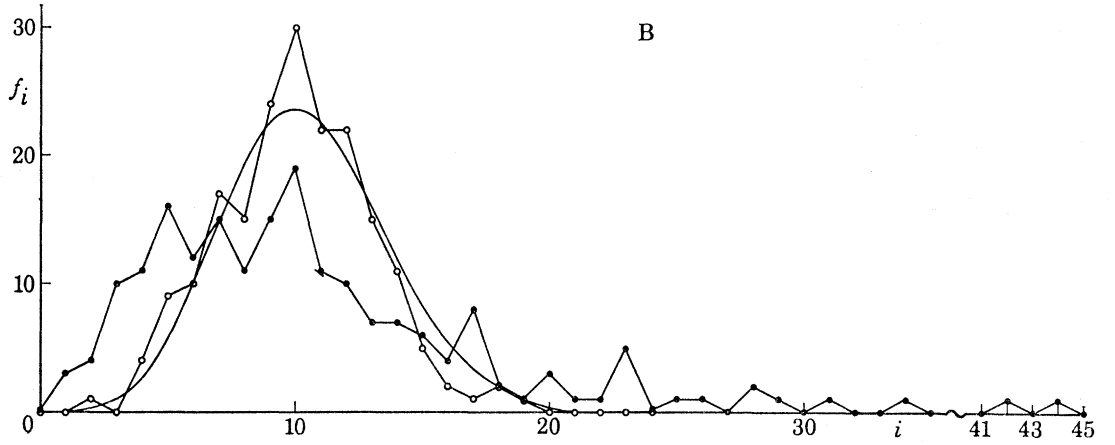

FIGURE 28. Comparison of square counts of the original (•) and simulated (○) area B with the theoretically derived Poisson curve (—). The symbol f_i is the number of areas observed or predicted to contain i craters.

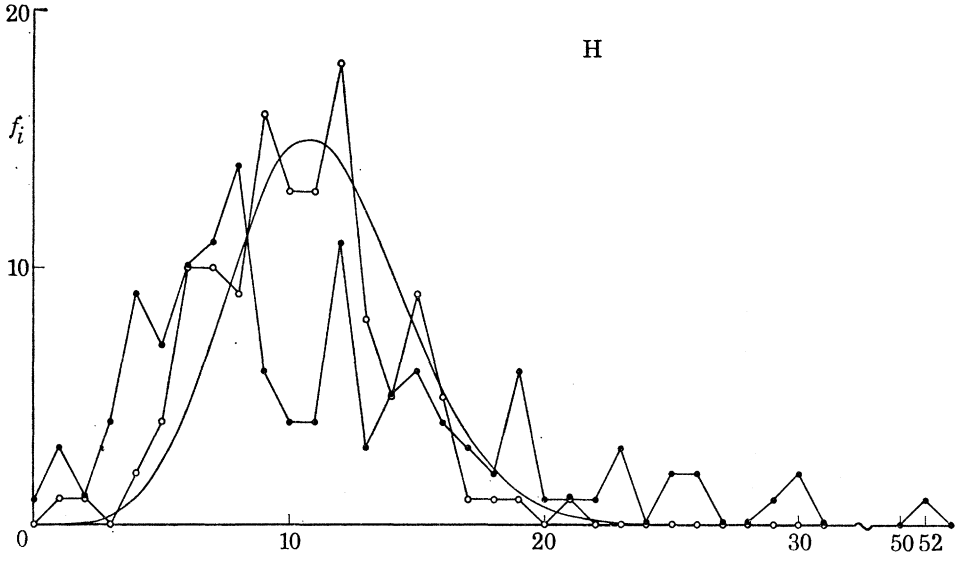

FIGURE 29. Comparison of square counts of the original (•) and simulated (○) area H with the theoretically derived Poisson curve (—). The symbol f_i is the number of areas observed or predicted to contain i craters.

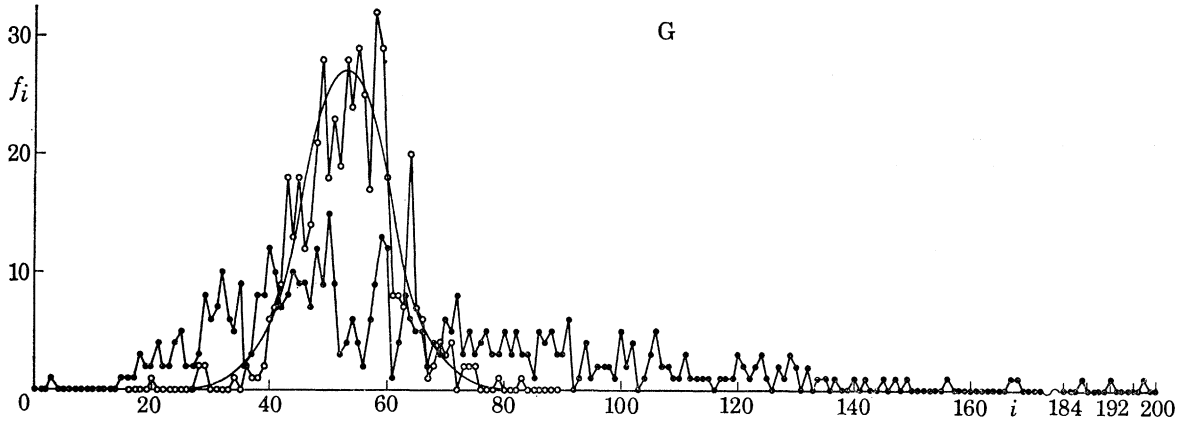

FIGURE 30. Comparison of square counts of the original (•) and simulated (○) area G with the theoretically derived Poisson curve (—). The symbol f_i is the number of areas observed or predicted to contain i craters.

greatly from the form of a random distribution and the type of departure is such that, on the Moon, many elemental areas have fewer craters than expected and many have more craters than expected on the theory that the craters are of primary impact origin. In other words, the craters in each of the three test areas cluster to a marked extent.

The amount and degree of clustering may be judged from figures 22, 24 and 26, respectively; and it may be compared with the 'accidental clustering' in the appropriate simulations. In all

TABLE 4

area	range of diameter/km	N	k	ν	χ^2 (simulated distr.)	χ^2 (actual distr.)
B	0.50 to 11.5	2001	191	12	10	269
H	0.10 to 6.6	1440	128	12	20	172
G	0.13 to 9.5	28356	496	38	68	>5600

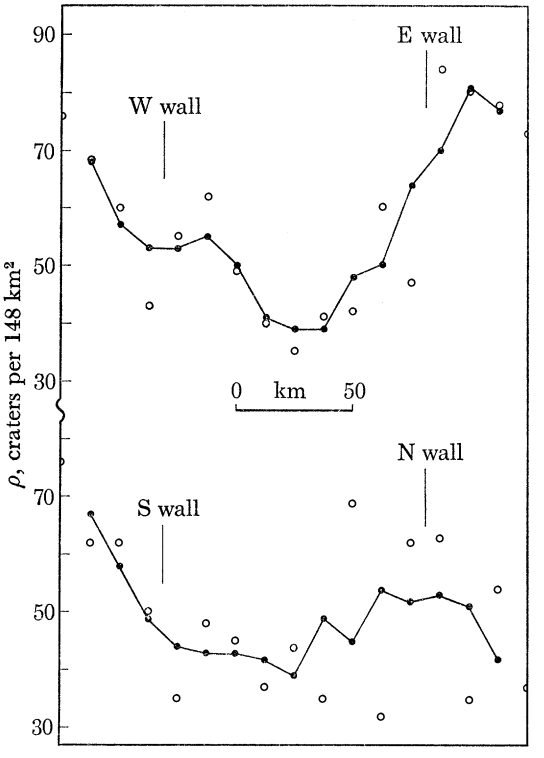

FIGURE 31. Variation of number density with position across Flamsteed P for the areas shown in figure 24. The open circles correspond to the original counts, the solid circles to a three-point running average.

three areas contours have been drawn to enclose regions having twice (and, where appropriate, higher multiples of) the mean number density, ρ. In each of the three fields the clustering is strong in comparison with the accidental clustering in a field of randomly placed points.

We note that the clusters of craters isolated by both the photometric method and by the square counting method bear no apparent relation to the largest craters in their vicinity. Such a relation might be expected were the craters in clusters a result of secondary impacts. The separation between centres of secondary craters would increase with the flight path of the secondary particles

and, for the rather tightly packed clusters we have been considering, it would seem inappropriate to look far afield for the source of secondary ejecta.

In area G (figure, 1) all the clusters of high number density occur outside the Flamsteed P complex, the ridges of which are shown as broken curves in figure 24. One of the photometrically derived clusters occurs on the NW rim of Flamsteed P. The mean number density of craters within Flamsteed P is only 50 craters per 148 km^2, whereas it is 60 per 148 km^2 for the entire field. Again, the photometric method shows the interior of Flamsteed P to have an exceptionally low

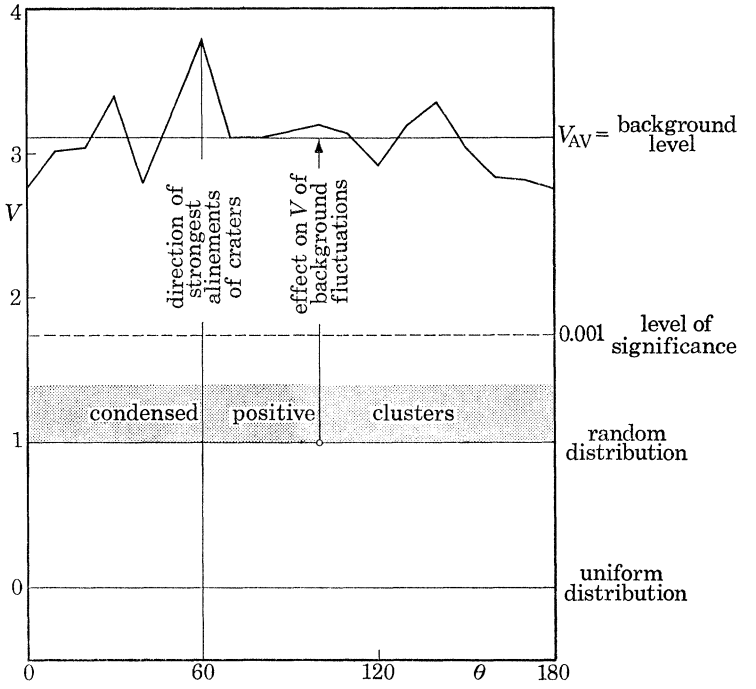

FIGURE 32. Idealized (V, θ) diagram (see text).

fractional area covered by craters. Possibly the floor of Flamsteed P is more recent than other parts of the field. Indeed, smoothed W to E and S to N profiles of crater number-density, ρ, taken across the ring-complex in the rectangular zones outlined in figure 24 show sharp rises in ρ as the west, east and south walls are traversed in the positive radial direction (figure 31). There is no such significant change in ρ as the north wall is traversed, but this is because the ridges bounding Flamsteed P open out, on the north, giving the structure a 'breached' appearance. The northern terrain is therefore to be identified with the main floor of Flamsteed P. The generally high crater density in the SW part of area G appears to be limited on the Flamsteed side by a prominent wrinkle ridge. In area G, therefore, we can argue that at least some of the clustering of craters may be due to selective obliteration by volcanic flows. This argument for volcanism is independent of the origin of the craters counted: volcanic flows may or may not be accompanied by endogenic cratering.

Several of the clusters that occur in area H appear to be linked with the Lamont complex of wrinkle ridges. The position of the inner ring of Lamont is marked with a broken curve in figure 26 and some of the smaller clusters of large craters (enclosed by contours in figure 25 rather than in figure 26) coincide with this ring. An outer ring (not shown) contains some of the other clusters. Furthermore, several of the craters in clusters lie in linear arrays, as though controlled

by underlying fractures. It appears, therefore, that at least part of the clustering we have found in area H is a result of endogenic cratering.

3.5. *Separation of craters into types*

In the foregoing paragraphs we have demonstrated that strip tests may be devised and applied in such a way that it is possible to measure both alinements and clustering of craters. The reduced observations are presented in the form of (V, θ) polygons (figures 33 to 39), in which V is the

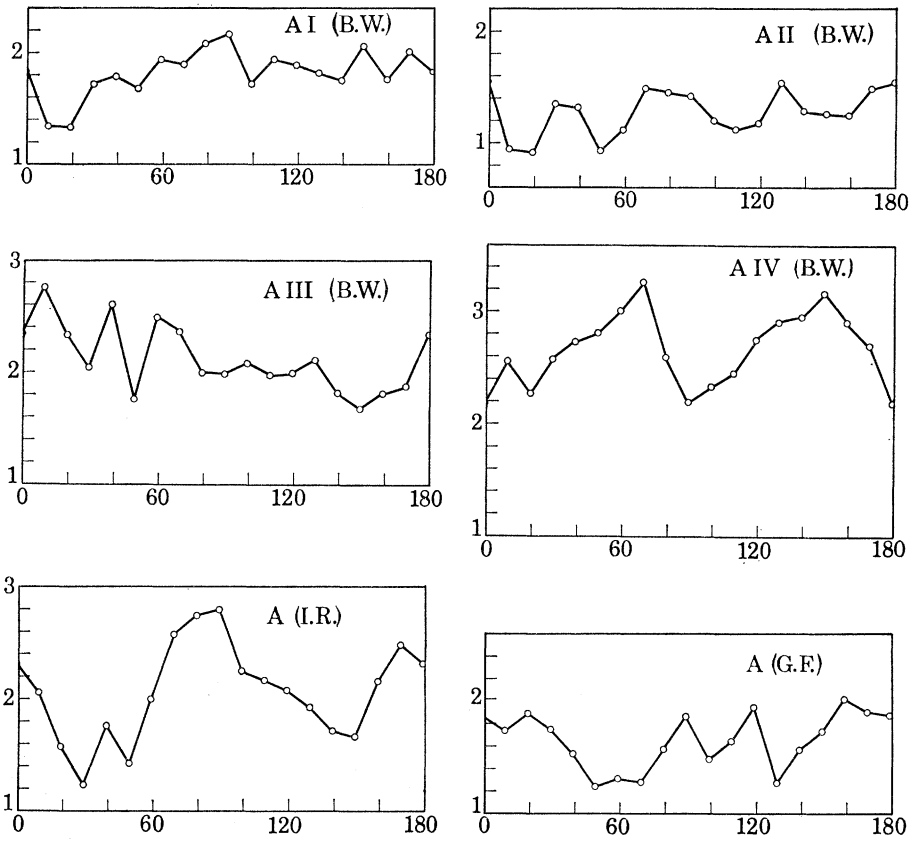

FIGURE 33. (V, θ) diagrams for various cartographers and subdivisions of area A.

computed index of dispersion and θ the position angle measured from selenographic north through east in a plane that is tangential to the centre of a test area.

The test areas themselves are, in general, very large (figures 1 to 4 and table 2). Their extent relative to the size of the largest craters with associated subradial arrays of crater chains is so great that any peak in V cannot, in general, result from subradial chains. Rather, our sampling technique ensures that a peak in V indicates parallelism of crater chains over the whole test area and, therefore, that the craters forming these chains are predominantly fracture-controlled (endogenic) craters not associated with subradial families stemming from parent craters.

Because of their size relative to the radius of the Moon, all test areas depart from plane surfaces and azimuths measured assuming the test areas are plane are in error by a small amount. Even in the case of the largest test areas, the error in θ does not exceed a degree or so; and as, in any case, we accept a low resolution in azimuth, we do not correct this slight error.

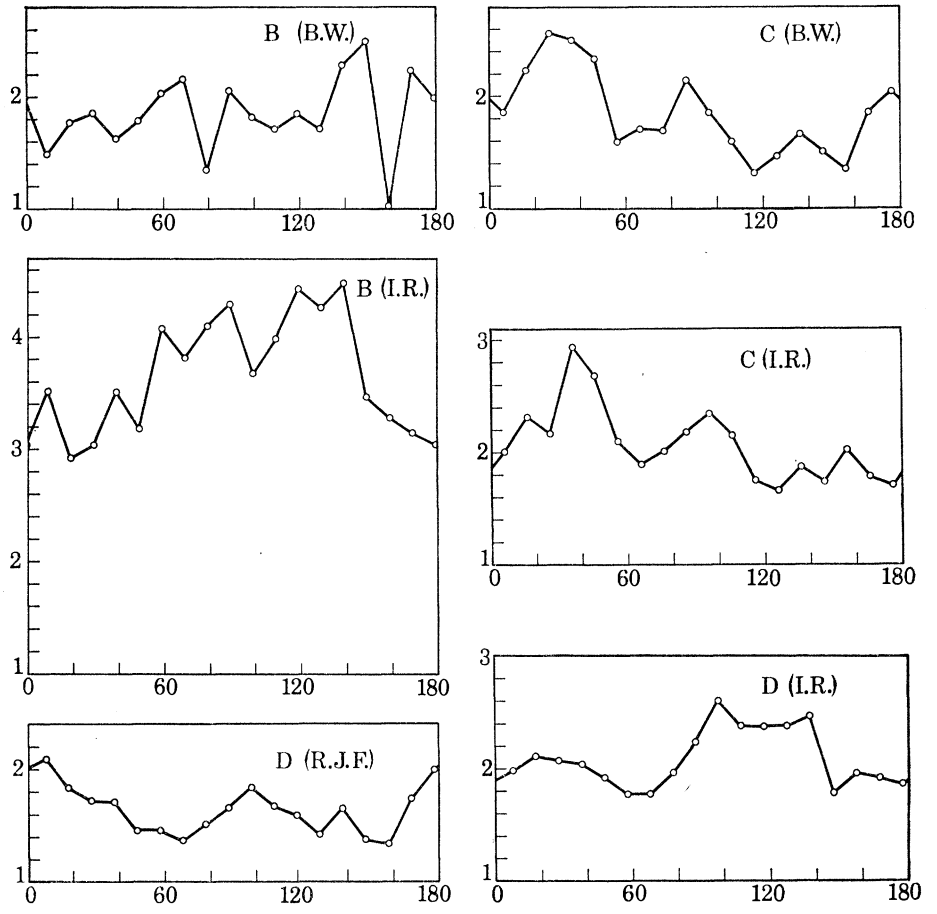

FIGURE 34. (V, θ) diagrams for various cartographers of areas B to D.

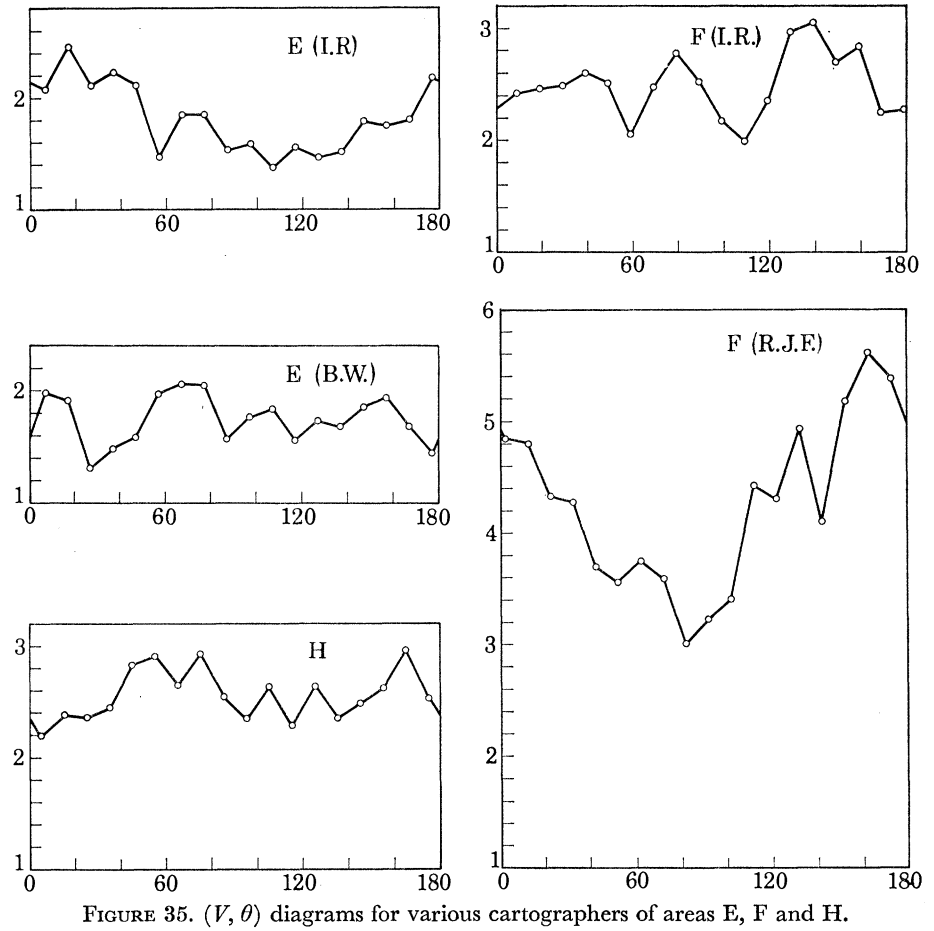

FIGURE 35. (V, θ) diagrams for various cartographers of areas E, F and H.

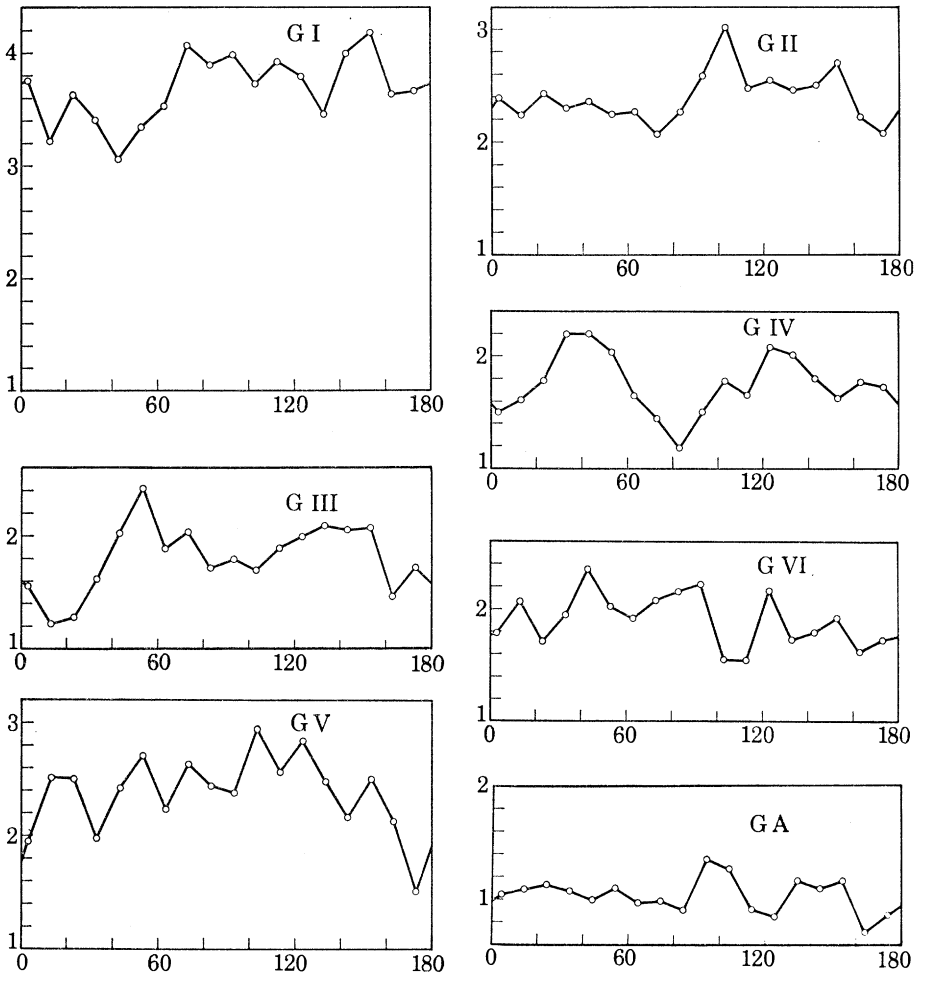

FIGURE 36. (V, θ) diagrams for various subdivisions of area G.

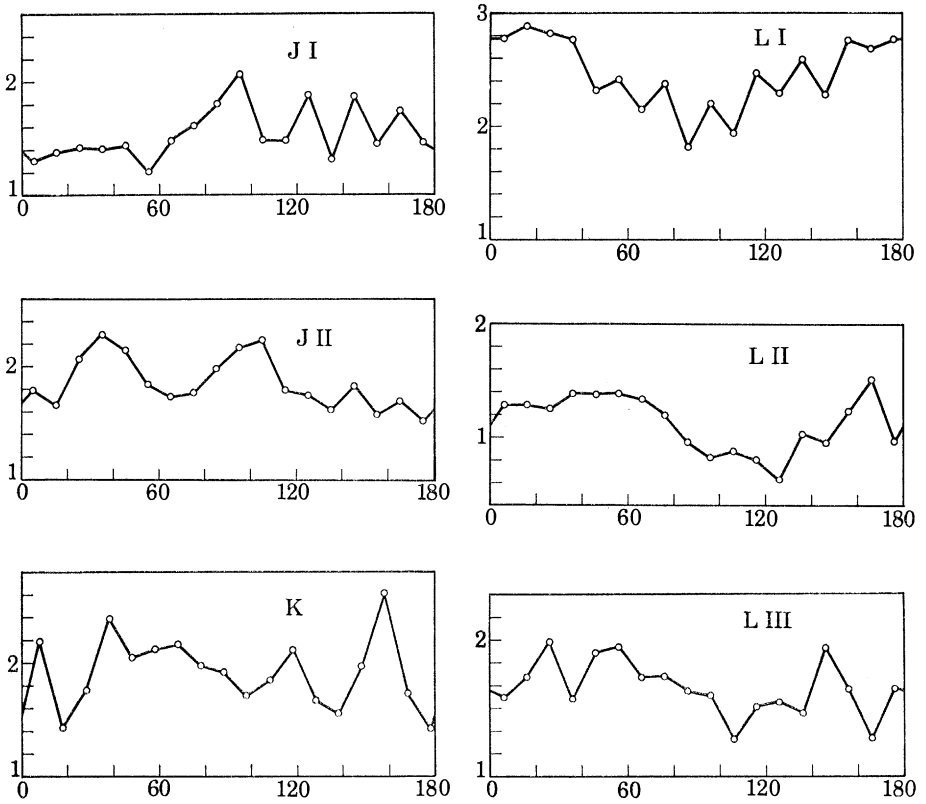

FIGURE 37. (V, θ) diagrams for various subdivisions of areas J to L.

Explanation of the interpretation of the (V, θ) diagrams will be aided by reference to an idealized figure (figure 32). The level $V = 0$ corresponds to a regular (uniform) distribution and the level $V = 1$ corresponds to a random distribution of crater centres. Only rarely do our (V, θ) polygons scatter around $V = 1$; commonly, they scatter around a significantly higher level. χ^2 tables are used to find the value of V that corresponds to the 0.001 level of significance for

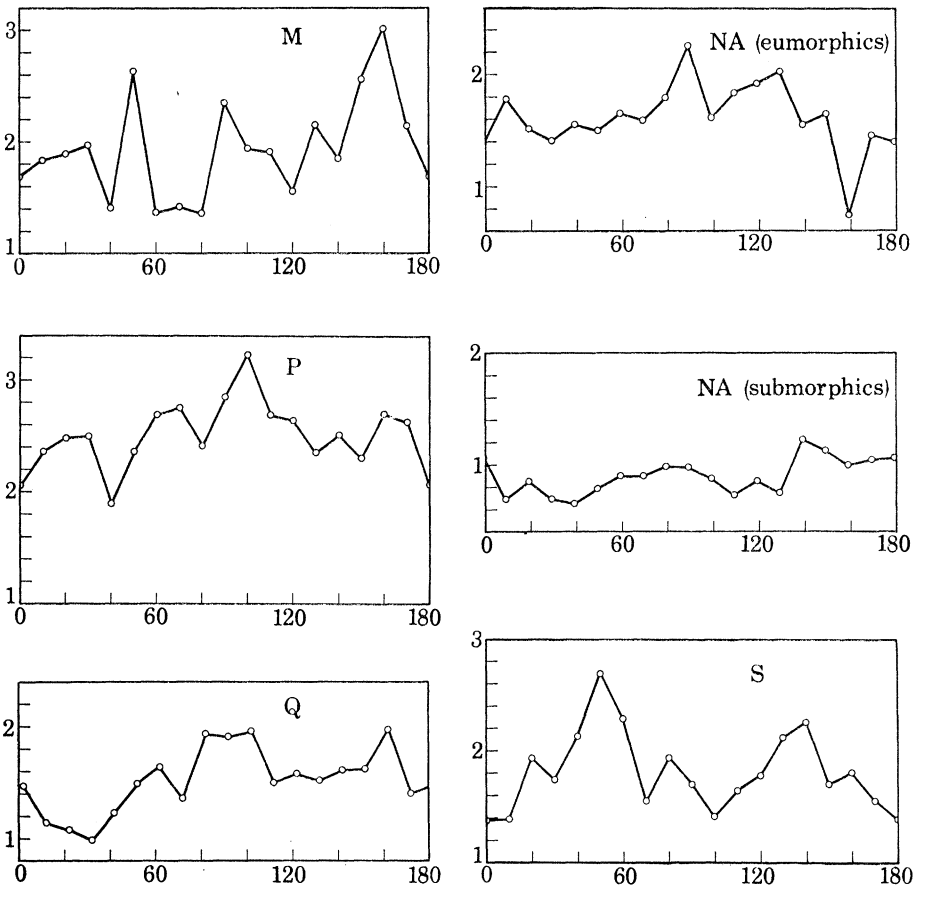

FIGURE 38. (V, θ) diagrams for the areas M, NA, P, Q and S.

49 degrees of freedom (the number of strips having θ = constant, minus one): this value is $V = 1.74$; and peaks not attaining this V-value are not used in the estimation of the proportion of craters in chains. Application of the level $V = 1.74$ to each of our (V, θ) diagrams shows that, in most cases, their average V-value exceeds the adopted level of significance.

The first conclusion that emerges from the (V, θ) diagrams, therefore, is that the lunar craters in the size bracket from 100 m to a few kilometres in diameter are generally non-randomly distributed. This corroborates the results drawn from the photometric and square counting methods. The non-randomness is exhibited in the form of clustering or chaining of craters. The eye tends to pick out 'positive' clusters of craters; that is, exceptionally high number densities of craters in elemental areas. However, 'negative' clusters, that is, elemental regions where there are few or no craters, are equally important in yielding high V-values.

Tests were made in an attempt to segregate the contributory sources of high V-values. On each

of six of the 22 test areas four of the densest positive clusters were measured for cluster density, ρ_c, defined as the number of cluster craters per square centimetre of photographic print.

The results are given in table 5 in which $\bar{n}$, the mean number of craters in a cluster, the mean cluster density, $\bar{\rho}_c$, and the mean crater density, $\bar{\rho}$, for the whole field are noted. The quotient $\bar{\rho}_c/\bar{\rho}$ defines a parameter that may be called the 'cluster coefficient'. It is seen that the cluster

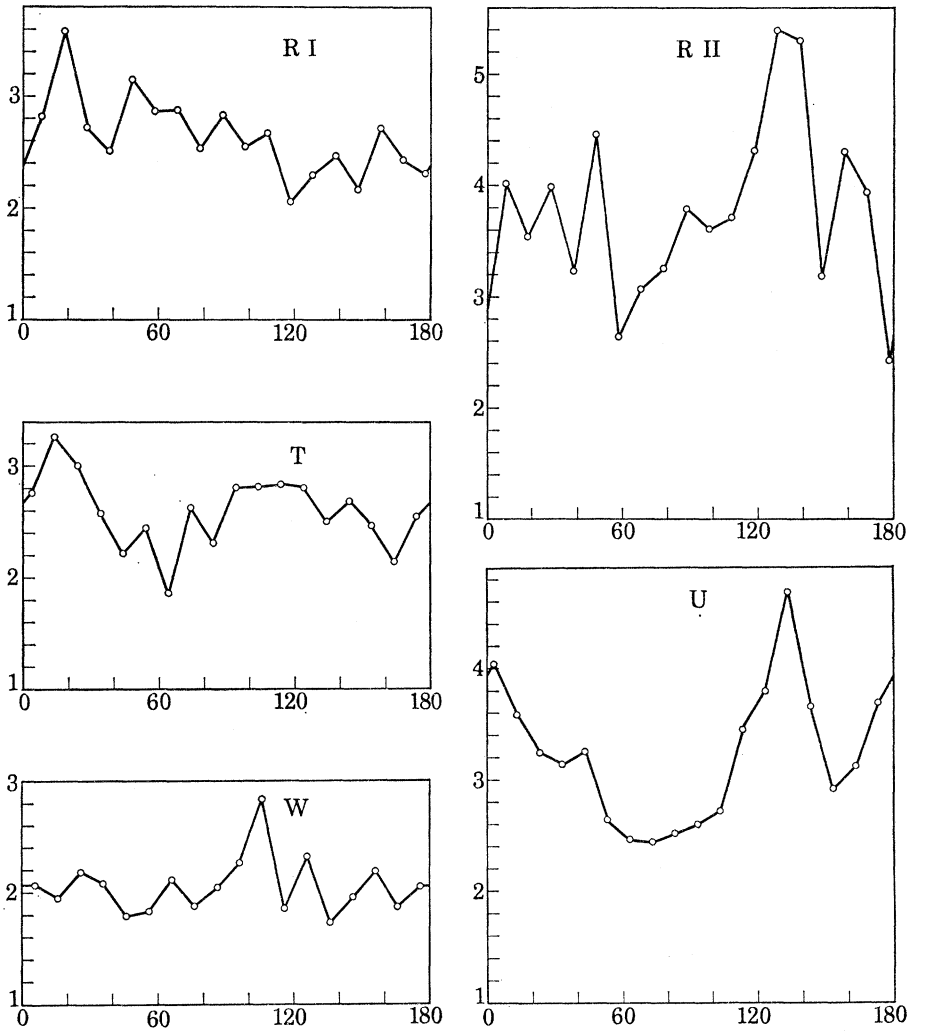

FIGURE 39. (V, θ) diagrams for the areas R (I and II), T, U and W.

coefficient varies from 2.1 to 6.7 for cases which were selected because they were thought to represent extremes. Next, three fields of random points were prepared, using the 1130 computer, and positive clusters were superimposed on these random fields.

A variety of artificial clusters with $\bar{n}$ taking the values listed in table 5, in turn, were given circular boundaries, their radii lying in the range computed to give precisely the range of cluster coefficients encountered in the original measurements (table 5). The number of clusters of each radius was changed from one simulation to the next in order to cover the whole range of clustering, from small numbers of clusters per unit field to large numbers of clusters per unit field, realized in all the test areas.

Strip tests were performed on these three simulations. As before, blocks of five strips calculated

to have an average of five craters per strip were placed in ten random positions to obtain 50 strip counts parallel to a given azimuth. Because the artificial clusters were circular, it was unnecessary to change the azimuth in subsequent tests: any one azimuth gave the same result as any other, apart from sampling fluctuations. Errors due to sampling fluctuations were minimized by repeating the test.

Even in the case of the highest amount of positive, condensed clustering attained in our test areas on the Moon the V-value, derived from simulations having an equivalent amount of

TABLE 5. CLUSTER DENSITIES AND CLUSTERING INDICES

	area					
	B	D	E	G	J	L
$\bar{n}$	19	20	14	100	28	56
$(\rho_c)_1$	2.8	3.4	2.7	25.4	3.7	2.3
$(\rho_c)_2$	3.4	2.4	4.2	24.8	4.9	2.5
$(\rho_c)_3$	3.4	2.1	2.2	23.8	6.0	2.0
$(\rho_c)_4$	3.3	3.4	2.4	22.9	4.7	4.6
$\bar{\rho}_c$	3.2	2.8	2.9	24.2	4.8	2.9
$\bar{\rho}$	0.56	0.66	0.43	11.47	0.99	1.31
$\bar{\rho}_c/\bar{\rho}$	5.7	4.2	6.7	2.1	4.8	2.2

clustering, was found to be only 1.4. Thus it appears that the highly condensed clusters of lunar craters that may be isolated so easily by eye have relatively little effect in raising the V-value of a random distribution above unity. The range of V in which the condensed positive clustering effect operates is stippled in figure 32.

Examination of photographs of areas known to have generally high V-values, and tests on artificial distributions of points, leaves no doubt that the overriding cause of the general elevation of V is to be found in background fluctuations of number density. Peaks in V over and above this 'background level' are due also to crater alinements in the direction in question. Therefore a peak such as that at 60° in figure 32 has a V-value resulting partly from cratering in chains and partly from the non-random cratering of the background. The background fluctuations in number density will now be discussed in more detail.

Background fluctuations are found to fall into one of two broad categories: they are (*a*) diffuse (positive or negative) clusters of craters or (*b*) systematic changes in ρ across a field. Category (*b*) fluctuations may be either (i) gradual or (ii) abrupt. In some areas, for instance, the mean crater density changes abruptly across a mare ridge.

Category (a) fluctuations. We can discuss four possible causes of diffuse clustering of craters. One is that they are secondary impact craters from sites distributed over the whole lunar surface. Walker (1967) has claimed, on the basis of theoretical calculations, that secondaries do not contribute significantly to the Moon-wide statistics for craters larger than 100 m in diameter.

A second possible cause of diffuse clustering of centres is to be found in the theory that the regolith varies in thickness with selenographic position. By regolith we mean a layer of fragmental rock, produced by meteoric impacts and gravity flowage, detached from an underlying layer of solid rock. McCauley (private communication, 1968) has proposed that, since solid rock would transport seismic energy much more efficiently than the regolith, craters would tend to disappear relatively quickly from areas of thin regolith. In areas of thick regolith, the seismic coupling between craters would be poorer and craters would tend to persist in the eumorphic form for a longer time. On this hypothesis one can imagine a large, old impact crater, filled with regolith,

to have a positive cluster of craters within the confines of its rim. The regolith hypothesis would predict negative clusters in those places where the hypothesized underlying rock approached the surface; such a situation would occur only where no large, ancient craters had been formed and filled with regolith alone.

The hypothesis may be subjected to tests that are, however, beyond the scope of this paper. For example, is there a relation between crater morphology and crater size for a given region (see Oberbeck & Quaide 1967), and does this relation change systematically between regions of positive clustering and regions of negative clustering? One simple test that may be made here argues against the hypothesis: the floor of Flamsteed P has a low crater density relative to the surrounding country (figure 24), the reverse of what one would expect on the regolith hypothesis. Again, relatively intense clustering of craters is found in the outer-rim regions of Flamsteed P, Lamont, and other ring structures; and the regolith hypothesis would require these regions to have a lower number density than the surroundings. We conclude that category (*a*) fluctuations are not solely a result of differing thickness of regolith.

A third possible cause of the fluctuating number density of the background is that a certain proportion of the craters are volcanic and that these craters tend to be limited to the most active regions.

A fourth possible cause of category (*a*) fluctuations is to be found in the blanketing effect of volcanic flows. No matter what the origin of the craters, a late volcanic flow will cover craters and leave a negative cluster. We have clear evidence that volcanic flows have occurred in several of the areas we have studied and therefore, of the four hypotheses, we consider this one to be apt.

Category (b) fluctuations. (i) Gradual systematic changes in the number density of craters across an entire test area have been encountered in a few instances. We can explain these changes on the hypothesis of a regolith with systematically varying thickness but it is difficult to see how such a regolith could develop. Partial blanketing of craters by ejecta from some site or sites outside the area does not seem plausible. Differential volcanic cratering on a background of impact craters and volcanic flows again seems to provide the most logical solution.

(ii) Observations of abrupt changes in the amount of cratering apparently yield to one decisive solution of the problem. Abrupt changes occur along a physical boundary such as a ridge or, possibly, a fracture. First, one may conceive of a fracture intersecting the Moon's surface in a linear trend that separates a region of thick regolith from a region of thin regolith. It follows that ρ would be expected to change abruptly from one side of the fracture to the other. A serious difficulty would be to explain why the regolith differed sufficiently in thickness across the fracture.

Secondly, where the abrupt change in ρ occurs across a wrinkle ridge which is known to be associated with a source of lavas, there can be no doubt that the lava flow and volcanic cratering hypotheses provide the most reasonable solution to the question. Adopting this interpretation, the latest lavas would have flowed unilaterally from the ridge and would have covered pre-existing craters. Additionally, volcanic cratering could differ in intensity from one flow to another. Several cases with independent evidence for unilateral flow from mare ridges are known.

In conclusion, it appears that both category (*a*) and category (*b*) fluctuations in number density may best be explained on the hypothesis of differential blanketing by lava flows that may or may not sport endogenic craters. We believe, therefore, that volcanic patchiness in a mare area is an important contribution to the 'background level' of V (figure 32).

It is worth noting that if volcanic cratering or lava flooding are major contributors to the observed non-randomness, then a relation between clustering and size of crater might logically

be expected. The investigations were made using maps of the position of all craters greater than the accepted minimum diameter and the problem of size dependence on clustering could not in general be investigated. Limited investigations were possible where two or more maps, with different minimum diameters, had been prepared during the course of other investigations. These cases are discussed in § 4.2.

4. Interpretation of individual (V, θ) diagrams

4.1. *Separation indices and method of separating clustering from chaining*

In order to interpret any particular (V, θ) diagram it is necessary to consider (*a*) the range of separation index for the region in question and (*b*) a means of separating the effects of chaining from non-directional clustering.

(*a*) In the real case the separation index, S, will vary from one chain or cluster to another and from one part of a field to another. In the first instance, therefore, it may be assumed that the index is unity. This assumption is not unreasonable when the following two considerations are borne in mind: (i) separation indices much less than unity would result in chains that would be very prominent against the background; these are not, in general, observed; (ii) chains of increasing separation index have progressively less effect upon observed V-values. (Chains with $S \geqslant 5$ would be undetectable.)

A further refinement can be made to this estimate, to set acceptable limits to S. Clustering of craters in a field, coupled with the restricted number of positions in which blocks of strips were placed, resulted in the observed mean numbers of craters per strip differing slightly from the intended value of five. The spread of separation indices for each area was therefore taken to be the spread in the values of $5/\bar{N}$ for that area, values of $\bar{N}$ for each azimuth θ being used.

(*b*) The effect of non-directional clustering may, under certain assumptions, be removed. The (V, θ) curve for an ideal, 'purely chained' region lies close to the value $V = 1$, except in those cases in which θ lies along a chaining direction. When the effect of clustering is included the whole curve may, to a first approximation, be regarded as being raised uniformly through a distance that depends on the degree and type of clustering. Within the accuracy of the method employed here this distance may be taken to be V_{av}, the mean of V for all eighteen values of θ, minus one (the random level)—see figure 32. The proportion of craters in chains for any particular azimuth may then be estimated as the difference between that naïvely estimated from the height of the peak in that direction, and the proportion that would give the background level of the whole curve in a purely chained region. In each case proportions of chained craters were estimated for each principal chaining direction by interpolation between the curves in figure 15.

This procedure had the additional advantage of providing a numerical value of the amount of clustering in the region. It is emphasized, however, that, since this measure of the percentage of craters in clusters is obtained by comparison with a purely chained region, the amount of confidence to be placed in the measure is limited.

A difficulty in the determination of the number of chaining directions within a region arises, in some instances, from the fact that a peak corresponding to a given chaining direction will have a definite breadth. In the worst possible case a chain may lie at $\pm \arctan \frac{1}{5}$ to the azimuth of the strips, and still yield the same value of P. This natural breadth of the peak arising from the shape of the strips may be augmented by other mechanisms. Three of these are: (*a*) slight variations in azimuth of chains across a field or within the same region, (*b*) the presence of short, closely spaced

TABLE 6. FIRST ESTIMATES OF CLUSTERING AND CHAINING PERCENTAGES

area designation	Δ_{min}/m	V_{av}	S_{min}	S_{max}	$(P_c)_{min}$ (%)	$(P_c)_{max}$ (%)	θ	P_{min} (%)	P_{max} (%)	$(P_t)_{min}$ (%)	$(P_t)_{max}$ (%)
A (I.R.)	<700	2.05	0.87	0.98	24	29	89	13	24	52	61
							169	6	16		
A (G.F.)	700	1.64	1.06	1.14	19	22	19	5	12	52	63
							89	3	11		
							119	6	13		
							159	8	14		
A I (B.W.)	350	1.82	0.77	0.84	17	19	90	5	9	28	34
							150	3	7		
							170	2	6		
A II (B.W.)	350	1.27	1.08	1.20	10	11	0	7	10	28	34
							70	5	9		
							130	7	10		
A III (B.W.)	350	2.11	0.92	1.00	28	32	10	11	20	59	70
							40	7	15		
							60	5	12		
A IV (B.W.)	350	2.69	0.67	0.72	29	32	70	9	21	50	61
							150	6	13		
B (B.W.)	700	1.85	0.77	0.81	17	19	70	5	9	41	49
							90	2	6		
							150	12	16		
							170	6	10		
B (I.R.)	500	3.68	0.78	0.89	54	63	60	0	19	87	100
							90	4	23		
							130	7	25		
C (I.R.)	643	2.07	0.94	1.02	28	34	36	15	26	52	61
							96	0	10		
C (B.W.)	643	1.85	1.01	1.09	25	28	26	15	22	57	65
							56	0	3		
							86	5	10		
							176	3	9		
D (I.R.)	633	2.08	1.15	1.25	36	38	98	13	20	62	69
							138	9	16		
D (R.J.F.)	317	1.63	0.95	1.04	17	19	8	10	16	34	40
							98	3	9		
E (I.R.)	643	1.81	0.86	0.91	18	21	17	13	27	54	67
							37	8	14		
							70	−1	3		
							177	7	12		
E (B.W.)	643	1.75	0.92	0.98	19	21	7	4	7	36	45
							67	6	11		
							107	0	5		
							157	3	8		
F (I.R.)	634	2.50	1.01	1.14	41	48	40	−5	10	71	96
							80	1	15		
							140	7	22		
							160	3	16		
F (R.J.F.)	317	4.24	0.92	1.05	78	92	110	−8	15	100	100
							130	3	22		
							160	8†	22†		
G I (G.F.)	126	3.67	1.10	1.14	72	85	73	7	22	100	100
							93	6	21		
							113	3	20		
							153	9	24		
G II (G.F.)	126	2.39	0.95	1.05	36	40	103	11	26	58	71
							153	3	13		
G III (G.F.)	126	1.82	0.96	1.04	22	24	53	13	18	50	57
							73	5	8		
							133	7	12		
G IV (G.F.)	126	1.75	0.85	0.90	17	20	43	8	13	35	39
							123	5	10		
G V (G.F.)	126	2.36	0.58	0.64	21	23	23	1	5	47	59
							53	3	7		
							73	2	7		
							103	6	12		
							123	5	11		
							153	0	4		
G VI (G.F.)	126	1.91	0.74	0.83	18	21	13	0	6	38	49
							43	6	12		
							93	3	9		
							123	2	8		

TABLE 6 (*cont.*)

area designation	Δ_{min}/m	V_{av}	S_{min}	S_{max}	$(P_c)_{min}$ (%)	$(P_c)_{max}$ (%)	θ	P_{min} (%)	P_{max} (%)	$(P_t)_{min}$ (%)	$(P_t)_{max}$ (%)
GA	126	1.06	0.85	0.93	0	0	93	8	10	8	10
H (G.F.)	100	2.55	0.85	0.92	35	38	55	5	12		
							75	6	13		
							105	−1	5	64	78
							125	−1	5		
							165	6	14		
JI (R.J.F.)	405	1.54	0.86	0.93	12	14	95	11	16		
							125	7	11	44	53
							145	6	11		
							165	3	7		
JII (R.J.F.)	405	1.80	0.94	1.01	21	24	35	9	15	43	48
							105	8	14		
K (G.F.)	670	1.91	0.72	0.80	17	20	8	3	9		
							38	6	13		
							68	2	8	51	64
							118	1	7		
							158	10	17		
LI (R.J.F.)	320	2.47	1.06	1.48	42	60	16	−5	33		
							36	−8	29	65	100
							156	−8	29		
							176	−8	29		
LII (R.J.F.)	320	1.13	0.87	0.94	2	3	6	4	6		
							26	4	6		
							46	7	9	31	41
							66	5	8		
							166	9	12		
LIII (R.J.F.)	320	1.57	0.68	0.72	10	12	26	6	9		
							56	5	8	28	34
							146	4	8		
M (R.J.F.)	335	1.97	0.94	1.12	25	32	50	9	26		
							90	2	17	79	100
							130	−2	11		
							160	19	36		
NA (e)	116	1.62	0.79	0.88	13	15	9	1	9		
							89	11	17	38	47
							129	7	12		
NA (s)	116	0.90	0.83	0.89	0	0	139	5	6	5	6
P (C.T.)	360	2.52	0.82	0.88	34	36	70	4	7		
							100	12	18	58	65
							160	1	6		
Q (B.W.)	380	1.52	0.86	0.91	12	13	62	2	4		
							82	9	12	43	51
							102	9	12		
							162	8	11		
RI (B.W.)	703	2.64	0.88	0.92	38	40	18	20	25		
							48	11	15	82	90
							68	5	9		
							88	3	7		
RII (B.W.)	703	3.76	0.95	1.13	71	80	8	−5	21		
							28	−5	21		
							48	11	29	100	100
							130	20†	29†		
							158	4	20		
S (B.W.)	650	1.82	0.79	0.86	17	19	20	0	5		
							50	16	21	45	54
							80	0	5		
							140	6	12		
T (B.W.)	460	2.58	0.91	1.07	38	46	14	9	28		
							94	−2	15	60	91
							114	−2	16		
							144	−5	12		
U (B.W.)	685	3.20	1.01	1.18	60	71	3	8	35	100	100
							133	26	40†		
W (B.W.)	663	2.05	0.97	1.23	29	36	26	−4	12		
							66	−5	10		
							106	12	33	58	94
							126	−1	16		
							156	−4	11		

† For these peaks the initial value of (P_c+P) was apparently greater than 100 %.

chains (by a variation of the arctan $\frac{1}{5}$ effect), (*c*) the presence of elongated clusters or 'belts' of craters rather than 'pure' chains. It is possible to visualize additional mechanisms that would have the effects of broadening a peak on the (V, θ) diagram. As a first approximation we analysed only those peaks that were mutually separated by $\geqslant 20°$. In the appropriate cases, broad peaks were treated as being compound, and V-values read at 20° intervals were used in the analysis. Intersection of broad chains of craters were found to be so uncommon that we were able to ignore any increases imposed on the calculated percentages P as a result of particular craters contributing to chaining in more than one direction.

Table 6 summarizes the data so obtained, P_c being the estimated proportions of craters causing clustering alone, P the proportion giving rise to chaining alone and P_t the total estimated proportion of endogenic craters, based on the values of P_c and P.

4.2. *Discussion of individual areas*

Area A (figure 33, figure 1)

The difference between the values of V_{av} of areas A (I.R.) and A (G.F.) is due to I.R.'s having included smaller craters than G.F. (see § 3.2). The greater clustering (about 27 %) of craters in

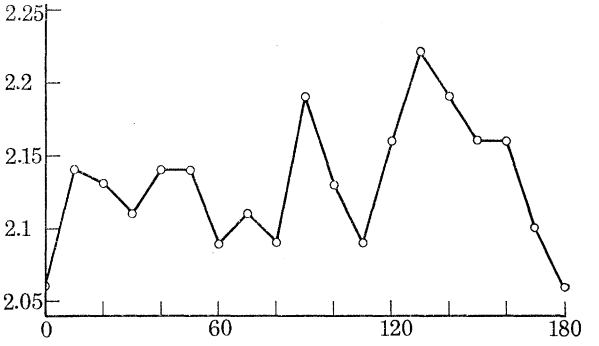

FIGURE 40. Mean (V, θ) diagram for all 41 areas shown in figures 33 to 39.

the I.R. map is, in fact, a direct result of its containing some 400 craters smaller than 700 m in diameter. If variations in photographic quality can be ruled out in this case—and we believe they can—these small cluster craters must be of internal or secondary impact origin. They cannot be 'islands' left by lava flows since, in that case, the larger craters would cluster in like fashion. For the same reason, it may be difficult to explain them in terms of varying thickness of regolith. Thus, in analysis of craters of different size in a given area we have a tool for separating out some of the hypotheses developed in § 3.5.

When area A is broken down into four parts, it is evident that the most intense clustering and chaining occurs in sections III and IV. The Orbiter photograph IV-H-127 shows that parts of sections III and IV are covered by wrinkle ridges and lava flows with well-developed fronts. The number density of craters is higher on the stratigraphically more recent flows, and the only reasonable explanation is that the excess craters on the flows is due to endogenic activity. Even more striking is the fact that the strongest chaining peaks at $\theta = 10°$, 70° and 150°, respectively, run parallel to the trends of the wrinkle ridges. This confirms our earlier reasoning that our method detects chaining of craters that are fracture-controlled and proves that a large proportion of our craters both in chains and in clusters are indeed of internal origin.

When corresponding V-values for each of the six independent investigations of area A are averaged (figure 41), strong peaks appear at $\theta = 70°$ and 170°. The 70° direction is that followed

by the most extensive system of mare ridges within the area. A conspicuous crater belt traverses the northern half of the area at $\theta = 170°$. Because of edge effects the presence of this belt is not apparent in the appropriate subsections I and II. The direction of the belt is prominent in A (I.R.) but not in A (G.F.) and this again suggests that the smaller craters contribute substantially to chaining. Some of the chain craters lie in patches of ray material and this argues strongly for the internal origin of these rays. At least 50% of the craters mapped in sections III and IV of area A, and possibly as many as 70%, are endogenic.

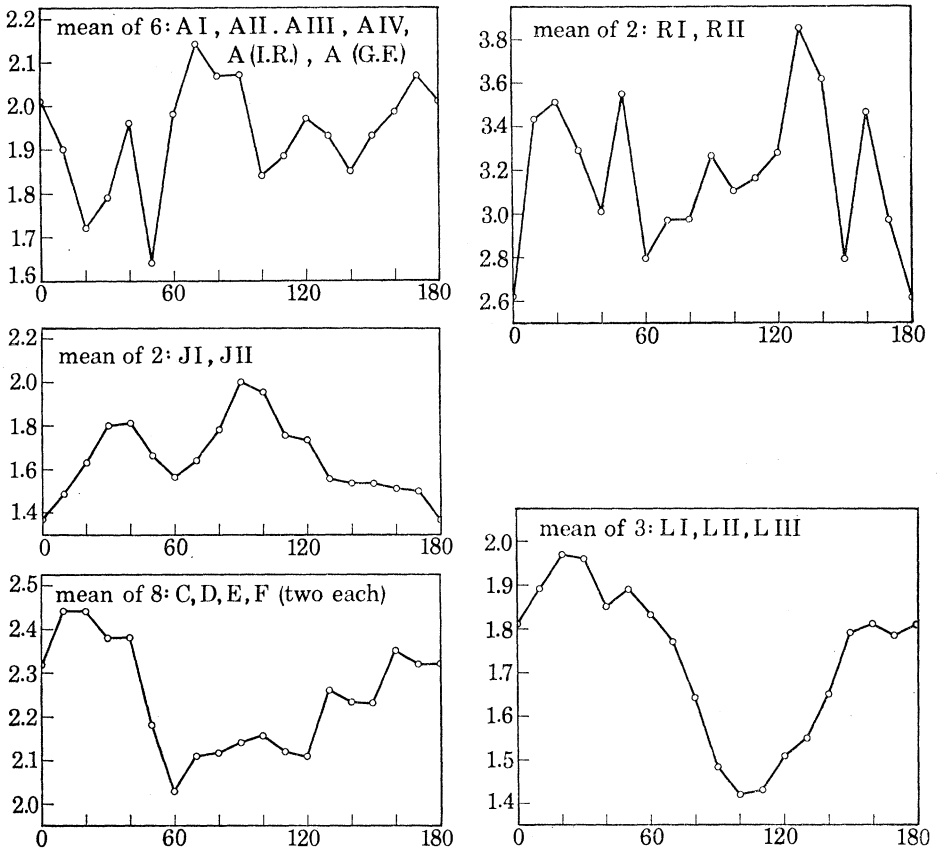

FIGURE 41. Mean (V, θ) diagrams for various subdivided areas.

Area B (figure 34)

The respective observers B.W. and I.R. measured craters down to 700 and 500 m or less in this area and, again, the 1080 smaller craters are much more clustered than the 950 larger ones. Thus, on the basis of clustering alone, up to 50% of the craters mapped could be of internal or secondary impact origin. A crater belt in the NW of the area appears to account for the 90° peak in V, and there is a parallel (west) trending mare ridge not far away in the NW corner of the area. The craters that generated this particular peak, at least, are confirmed to be endogenic. The strip tests suggest that the proportion of internal craters larger than 700 m is 41 to 49% and the proportion of internal craters larger than 500 m is 87 to 100%.

Area C (figure 34)

Again the value of V_{av} for C (I.R.) is higher than that for C (B.W.) and corresponds to an excess of 124 craters less than 643 m in diameter. These small craters cluster more than the larger

ones. Wrinkle ridges in this part of Mare Serenitatis trend at about 40° and 85°, and these directions coincide with two of our chaining directions. The well-known ray that passes close to Bessel is manifested as a broad peak centred on 25 to 30°. We estimate from C (I.R.) that between 52 and 61 % of all craters are endogenic; and from C (B.W.) the corresponding figures are 57 and 65 %.

Area D (figure 34)

This is the only area tested in which the background level of V is lower for the smaller craters. The result is almost certainly erroneous since it can be traced to an important sampling difference: an unusual cluster of submorphic craters (see § 2.2) was sampled on D (I.R.) but not on D (R.J.F.). We of course attempted to minimize such sampling fluctuations. Nevertheless, on some occasions they will be present and individual estimates of chaining and clustering will be in error. For D (I.R.) we obtain endogenic cratering of between 62 and 69 % and for D (R.J.F.) between 34 and 40 %.

Area E (figure 35)

The two areas E (I.R.) and E (B.W.) differ but little in the value of V_{av}. About 20 % of the craters are clustered in each case. More craters are chained in E (I.R.) (35 to 48 %) than in E (B.W.) (16 to 25 %) and the difference is due to sampling fluctuations. One may estimate that the chain craters form 16 to 48 % of the total, and that all endogenic craters attain 36 to 67 % of the total.

Area F (figure 35)

One observer (I.R.) measured craters down to 634 m and another (R.J.F.) down to 317 m. In the case of F (I.R.) $V_{av} = 2.50$ and for F (R.J.F.) $V_{av} = 4.24$—the highest background level encountered in any test. Again we have confirmation that the smaller craters have a large influence in raising the average V-value. Whilst a minimum of 71 % of the craters down to 634 m are estimated to be endogenic, the corresponding figure for all craters down to 317 m is 100 %.

Considering areas C, D, E and F together a broad peak, centred approximately on $\theta = 20°$, appears in the diagram (figure 41). This direction is most prominent in area C (figure 34) but it is present in areas D and E (figures 34 and 35). The direction coincides with the prominent ray that crosses Mare Serenitatis just west of Bessel.

Area G (figure 36, figure 1)

The subdivision of this area into six parts shows how the endogenic activity varies between adjacent fields. On average, the proportion of internally formed craters lies between 55 and 63 %. Strongly developed mare ridges traverse this region and correlations between their directions and those of crater chaining—especially at $\theta = 23°$, 73°, 103°, 123°, 133° and 153°—may be found. An independent investigation of a limited region adjacent, but external, to the north-east wall of Flamsteed P (Fryer 1968) also showed peaks at 23°, 123° and 133°. The peak at 123° was highly significant, the others less so.

The indicated proportion of internal craters is near zero inside the walls of Flamsteed P (see area GA) and, outside, is lowest to the north-west, towards which the walls of Flamsteed P open out. The implication of large-scale lava flows is inescapable. Flows from the wrinkle ridges present in all sections of area G may account for some of the apparent clustering present, and the estimated clustering proportions for the region are, therefore, probably too high.

Area GA (figure 36)

Craters in this area depart but little from random distribution. Clustering is nil though possibly† 10% of the craters are chained at $\theta = 93°$. Area GA is mainly representative of the interior of Flamsteed P. It is particularly interesting that the craters here should be randomly distributed for, if the interior of the ring has been covered by late flows (as suggested in § 3.4), that are relatively free of endogenic craters larger than 156 m in diameter, the flows would still register more recent impact craters. More than 90% of the craters in area GA may be of impact origin.

Area H (figure 35)

In this area, which covers the Lamont complex, about 37% of the craters are members of clusters and between 28 and 42% members of chains. Short chains that are conspicuous when the map of area H is viewed lie in the direction (165°) of the strongest chaining shown in the (V, θ) diagram.

Area J (figure 37)

Part I has a (V, θ) diagram with a strong peak at 95° and II has strong peaks at 35 and 105°. When the data for both parts are combined strong peaks remain at 35 and 95 (figure 41). Wrinkle ridges run through II at about 40°, 105° and 135°. Taken together, I and II indicate internal cratering amounting to between 43 and 53%.

Area K (figure 37)

Chaining in Mare Crisium is found at $\theta = 158°$, 38°, 8°, 68° and 118° (decreasing in strength in that order). A major system of mare ridges runs at about 155° and correlates with the principal chaining direction. This result could, of course, be explained if the ridges obliterated craters, leaving aligned clusters of craters between the ridges. However, just the reverse is true; the craters concentrate on the ridges themselves. The evidence that these craters are of internal origin is therefore strong.

The peaks at 8° and 38° can be correlated with other ridges. Correlation of chaining directions with the polygonal 'walls' of Mare Crisium is poor. At least 45% of the craters mapped appear to be endogenic.

Area L (figure 37)

Mare Humorum was sampled in the three sections of this area and in area M. The area LI gives a somewhat erratic (V, θ) diagram and estimated values of P_t show a large spread. A mare ridge traverses L II at about 176° and the strongest peak in V occurs at 166°—sufficiently close in azimuth to be associated with the 176° trend. The general shape of the (V, θ) diagram for L III is similar to that for L II and for L I so that, when the three sets of data are combined (figure 41) strong peaks occur at about 35° and 160°. Mare ridge segments in the vicinity of these areas L II and L III strike at 44°, 140° and 177° and all these directions may be correlated with chaining directions. The proportion of endogenic cratering turns out to lie between 31 and 41% for L II and between 28 and 34% for L III.

† The peak on the V-diagram does not rise above the adopted level of significance.

Area M (figure 38)

The best developed segments of mare ridges in this area run at 50° and 120° and coincide with two of the four directions of chaining. Belts of crater chains parallel the 160° direction, which the strip test method isolates as the direction of the most concentrated alinements of crater centres. The direction $\theta = 160°$ coincides with one of the principal directions of chaining in area L, which is adjacent to M.

Area NA (figure 38)

This is the only area in which the number of submorphic craters was sufficiently high to warrant segregation of these craters from the eumorphic craters. The eumorphics show some

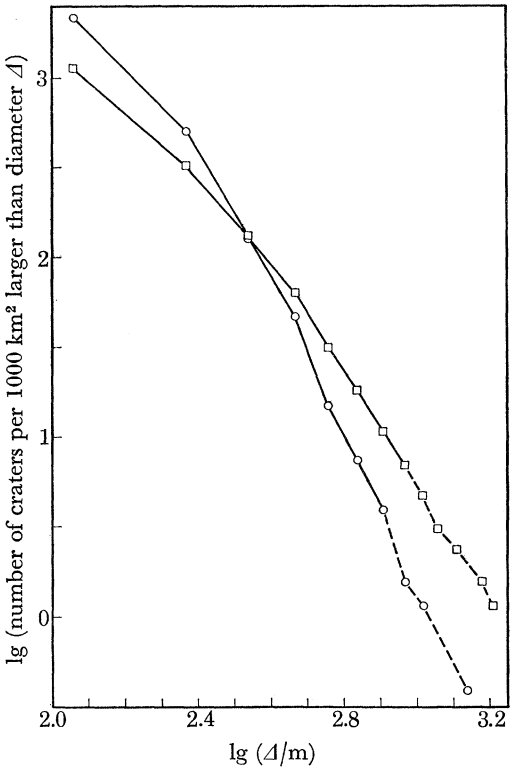

FIGURE 42. Comparison population curves for eumorphic and submorphic craters in area NA. □, Eumorphics; ○, submorphics.

clustering and they are alined along $\theta = 9°$, 89° and 129°. The submorphics do not cluster, even to the extent observed in a random disposition of points, and less than 6% of the submorphic craters lie in chains.†

A prominent flow front traverses part of area NA and, whilst the flow seems to have obliterated eumorphic craters, the distribution of submorphic craters is unaffected by it. At least one other flow front can be traced on the photograph. Possibly those eumorphic craters that are not members of chains are of impact origin. We are unable to explain the uniformity of the distribution of submorphic craters over the whole region: if they are of impact origin the distribution appears to be independent of the flows. Examination of the photograph shows that many of the

† This may not be a real chaining, since the peak lies below the adopted level of significance.

submorphic craters lie along shallow troughs that tend to follow the direction $\theta = 60°$ across the entire field. The troughs therefore appear to be tectonically controlled, and the submorphic craters may be interpreted as collapse depressions. The difference in the respective slopes of the cumulative plots of the eumorphic and submorphic craters (figure 42), if real, confirms that the two types of crater may form different populations.

Area P (figure 38)

Faint mare ridges run at about 70° and 95°, but the 100° peak is parallel to the direction of the framelets and we suspect that poor picture quality along the joins may, in this particular instance, introduce a spurious peak in this direction. If so, the figures for the extremes of P_t in table 6 should be reduced from 58 and 65% to 43 and 48% respectively.

Area Q (figure 38)

Of the four directions of crater alinement in this area only the 62° direction may be correlated with a lineament trend external to Tsiolkovsky. At least 40% of the craters may be endogenic.

Area R (figure 39)

This area contains a very complex system of ridges and lava flows, the latter originating beyond the south-east edge of Part II. The impossibly high limits on P_t are, therefore, entirely explicable in terms of lava patchiness and cannot be used for any estimate of true endogenic cratering. When parts I and II are combined (figure 41) chaining peaks persist at $\theta = 20°$, 50°, 130° and 160° and some flow ridging trends in each of these directions.

Area S (figure 38)

Lineaments in the vicinity of area S trend at about 50° and this is the strongest direction of chaining. Some lava flows of limited extent are apparent in the photograph, and a general increase in number density to the north must also contribute to the values of P_c which may, therefore, be overestimated.

Area T (figure 39)

A prominent mare ridge system runs at about 145° and this correlates with one of the four directions of chaining. Unpublished measurements by R. G. Strom of the trends of crater chains, elongated craters and ridges immediately SE of Taruntius, close to the present area, give peaks at 0°, 45° and 135° to 140°.

Area U (figure 39)

The high percentage of cluster craters in area U suggests that there is more than the average fractional extent of flows or volcanic craters in the area. This may be related to the general increase in number-density found in § 2.2 for the central region of the Moon's disk as it is approached along the central meridional belt.

Area W (figure 39)

Numerous mare ridges in this region trend at 45° and 150°. Of the four or five directions of alinement of crater centres only the 156° direction may be correlated with the trend of the ridges. This is the second area in which the chaining direction $\theta = 106°$ is thought to be spurious because

of variations in picture quality across framelets which run from east to west. Therefore, the limits of P_t should be reduced from 58 and 94 % to 42 and 60 % respectively.

5. Conclusions

5.1. *Improved clustering proportions*

In the light of the foregoing discussion of individual areas it is possible to refine the estimates of endogenic cratering. Since we so frequently find that the chaining directions across an entire

Table 7. Revised percentages of endogenic craters

area index	group	min. diam./m	area/km²	$(P'_t)_{min}$	$(P'_t)_{max}$
A	2	700	78790	44	55
AI	3	350	19698	16	22
AII	3	350	19698	25	31
AIII	1	350	19698	59	70
AIV	1	350	19698	50	61
B	3	700	84327	29	37
C	3	643	32367	49	57
D	4	633	19563	25	32
D	4	317	19563	16	22
E	2	643	32122	48	59
F	3	634	19079	41	66
F	2	317	19079	76	100
GI	4	126	12550	30	79
GII	4	126	12550	20	33
GIII	4	126	12450	27	31
GIV	4	126	12450	17	21
GV	4	126	10500	25	37
GVI	4	126	10500	19	30
H	2	100	36750	52	66
J	3	405	52054	29	43
K	2	670	47090	45	58
L	3	320	43213	21	91
M	3	335	17100	61	82
NA (e)	4	116	2582	24	33
NA (s)	1	116	2582	0	6
P	4	360	16103	24	31
Q	4	380	5906	31	39
R	4	703	39072	43	96
S	2	650	27927	39	48
T	3	460	15366	32	63
U	4	685	31673	48	67
W	4	663	37188	26	62

field are closely correlated with the directions of mare ridges known to be controlled by fractures it is clear that the percentage of craters in chains must be regarded as a lower limit on the proportion of endogenic craters. Although various types of crater may contribute to clustering we know that, in a few areas at least, clustering is due predominantly to the presence of endogenic craters. For example, smaller craters cluster more than larger ones in each of the areas A, B, C and F (that is, in four of the six areas (A to F) examined (§ 4.2) for dependence of P_c on crater size). Again, in area K, clusters of craters occur most commonly on broad mare ridges and the craters are thought to be of internal origin.

In general, it is not possible to eliminate secondary cratering, regolith variations and, especially,

lava patchiness from consideration as causes of diffuse clustering but, in those cases when the number density of craters changes monotonically across an entire field, endogenic cratering may be regarded as a major contributory factor in the change.

Therefore the maps of the individual areas were split into four groups (table 7) on the basis of their particular characteristic appearance. Group 1 contained those areas for which it was decided that no change in the first estimates of P_t was warranted. Group 2 contained those areas for which a small progressive change in ρ could be detected across a field. Group 3 contained areas having a marked progressive change in ρ; and group 4 contained all other areas—primarily those characterized by diffuse clusters but also a few with abrupt changes in ρ that probably resulted from obliteration of early craters by lava flows. A few of these group numbers were adjusted to be consistent with independent evidence for internal cratering discussed in § 4.2.

The clustering proportions, P_c, of table 6 were therefore recalculated, the contributions of diffuse clustering to the total P_t, being multiplied by 1, $\frac{2}{3}$, $\frac{1}{3}$ or 0, according to whether the area was assigned to groups 1, 2, 3, or 4, respectively. Whilst these factors tend to raise the minimum proportion of internal craters above the values deduced from chaining alone, we consider application of the factors to result in proportions of endogenic cluster craters that are deficient in numbers rather than in excess. The revised values of P_t, P'_t, are given in table 7.

It is seen from table 6 that, in the case of certain test areas, the proportion of endogenic craters tends to increase as the size of crater decreases. A similar effect might be expected when the limiting values of P'_t, weighted in proportion to the respective sizes of the regions from which the raw data were drawn, are averaged for various ranges of minimum crater diameter and mutually compared. To investigate this possibility we compared the average weighted P'_t, P''_t, for areas drawn from table 7 with minimum diameters $\geqslant$ 633 m, from 320 to 405 m, and from 100 to 126 m: the respective values of P''_t range from 37 to 52%, 33 to 63%, and 33 to 47%. The reason for the absence of the expected trend may be ascribed to the fact that, although the proportion of endogenic craters may increase with diminishing size in a given region, this trend may be marked by much larger differences in the proportion from region to region when an average is taken. Thus, considering the maria as a whole, it would appear that there was no dependence of P''_t on crater size over the range $100\,\mathrm{m} < \Delta \gtrsim 2000\,\mathrm{m}$.

Even though we have employed a high number of degrees of freedom in the index of dispersion tests, sampling fluctuations and other sources of input fluctuations have introduced a scatter in the results. A measure of the probable scatter in a particular case may be made from figures 16 to 20, in which 10% confidence limits have been recorded for V. The individual entries of P'_t in table 7 will contain built-in errors. Taken as a whole, however, their significance will be high. Because of the proved lack of dependence of P''_t on crater size, we are able to average all the limits (P'_t) min and (P'_t) max, respectively. Weighting each value of P'_t in proportion to the area of the region to which it refers, we arrive at the overall values (P''_t) min = 33%, (P''_t) max = 51%.

5.2. *Note on the absolute dating of units of lunabase*

The percentage $100 - (P'_t)$ min leads to upper limits on the number of primary impact craters in the lunabase. These figures, in turn, may be used to set upper limits on the age of each of the areas we have studied.

We adopt the law of particle influx which best represents all the relevant observations of the minor objects of the solar system in the vicinity of the Earth and we assume, in the first instance, that the same law of accumulation holds throughout the time of formation of the various lunabasic

units. The appropriate data have been marshalled by Vedder (1966) and he has proposed fitting them by means of the equation

$$\lg I = -14 - \lg m, \tag{15}$$

where I is the total number of particles of mass greater than m grams crossing 1 m^2 of cis-terrestrial space every second. We adopt $\Delta/15$ as representative of the diameter of a meteoroid, density 3 g cm^{-3}, which forms a crater of diameter Δ, and compute the mass required to form a crater of diameter Δ_{min}, listed in table 7. Application of equation (15) then leads to a value of I which may be used to compute the age, listed in table 8, of a particular region. Without weighting the results the average age of the areas studied is calculated to be between 2.2 and 4.5 Ga (Ga = 10^9 years).

Now the values of P_t' were calculated on the basis of ignoring cluster craters in group 4 areas; yet it does not follow that these cluster craters are all primary impact craters. Some, for instance, may be secondary impact craters or volcanic craters. Both the calculated limits of age are, therefore, overestimates.

Equation (15) is, itself, uncertain. The raw data on which it is based are sparse, show a large scatter, and do not extend far into the range of mass required to produce craters of the size encountered in this paper. Both the slope and the intercept of the line adopted by Vedder may be in error, in application to our data, by an amount sufficient to produce an order of magnitude change in the estimated ages. Furthermore, the flux of particles in the vicinity of the Moon may have been higher, in the past, than that deduced from modern observations and this would again lead to an overestimate in the ages. Some authors even believe that the present flux, corrected for observational losses, is ten times that given by equation (15). It is entirely possible, therefore, that the real ages are smaller than those calculated by an order of magnitude or more. Nevertheless, Fricker, Reynolds & Summers (1967) have deduced that the heating and volcanic activity (such as might have produced the maria) reached a maximum between 1 and 3 Ga ago, and these estimates are of the same order of magnitude as our calculated ages. Again it is noted that the deduced order of magnitude of the ages compares favourably with those measured by the ^{40}K–^{40}Ar method applied to igneous rocks returned from the Apollo 11 and 12 sites (3.7 and 3.4 Ga, respectively. The implication is that, if the flux given by equation (15) is adopted, there is no need to postulate a flux of meteoroidal debris that varies with time, in the size range considered.

Since the ages listed in table 8 are based on individual values of P_t' that scatter around the 'correct' values of P_t', the individual ages listed must contain errors in like fashion. Even relative ages of individual test areas are not, therefore, to be attributed high weight. However, the quoted ages may be regarded as giving some indication of the spread in the age of the different areas.

When the apparent ages of a given region are examined as a function of the diameter of the smallest crater mapped, as is possible for areas A, D and F, it is found that there is a large difference in the ages deduced separately for each area. These discrepancies may be interpreted as errors in the estimated proportion of endogenic craters for the regions in question. This implies that the age of any area relative to any other separately investigated area may be in error by a factor of at least two or three. Area A, when subdivided into four parts, shows apparent ages differing by factors of up to two. Comparison with the original photograph reveals that the apparently youngest area, A III, lies upon a recent lava flow with a well-developed flow front; the next youngest, A IV, lies on a less obvious flow; and the remaining two lie off the flows.

The apparently youngest areas are G I, G II, G III, H, L and M. The rings Flamsteed P and

Lamont, which Guest & Fielder (1968) have argued are young volcanic features, occur in areas G and H. Areas L and M are adjacent and together argue for the youth of Mare Humorum.

It is interesting to note that the floor of Mare Orientale is apparently the oldest of our areas. This area also has a high estimated proportion ($\geqslant 45\%$) of endogenic craters, and so the high apparent age is unlikely to have been caused by an underestimate of the proportion of endogenic craters present. On the other hand, many of the craters in Mare Orientale may be of secondary impact origin.

TABLE 8. ESTIMATED AGES OF INDIVIDUAL AREAS

area designation	min. age/Ga	max. age/Ga	'average' age/Ga
A (G.F.)	1.78	2.22	2.00
AI	5.01	5.26	5.17
AII	4.44	4.76	4.60
AIII	1.90	2.60	2.25
AIV	2.48	3.11	2.80
B	3.59	4.05	3.82
C	2.93	3.48	3.21
D (I.R.)	5.40	5.96	5.68
D (R.J.F.)	2.06	2.20	2.13
E	2.78	4.24	3.51
F (I.R.)	3.72	6.45	5.09
F. (R.J.F.)	0.0	0.486	0.243
GI	0.220	0.737	0.479
GII	0.728	0.870	0.799
GIII	0.826	0.872	0.849
HIV	1.06	1.11	1.09
GV	1.45	1.81	1.63
GVI	1.03	1.19	1.11
H	0.02	0.028	0.030
J	1.56	1.94	1.75
K	2.77	3.52	3.15
L	0.56	2.32	1.44
M	0.53	1.15	0.84
NA (e)	1.80	2.04	1.92
P	2.0	2.20	2.10
Q	7.84	8.87	8.36
R	0.47	6.70	3.59
S	9.18	10.80	9.99
T	5.38	9.89	7.64
U	4.77	7.51	6.14
W	3.20	6.24	4.72

5.3. *Tectonic implications of chaining directions*

If the directions in which the centres of craters are alined are indeed controlled by fractures, then one might expect the most significant directions of alinement, found by averaging all values of V corresponding to azimuths θ = constant, to be correlated with known tectonic lineaments. Maps of the lunar 'grid system' have been published by Fielder (1964) and Strom (1964). For the central regions of the lunar disk the principal directions of lineaments lie at = 135° (Fielder's 'system A', which is the best developed system of topographic lineaments), $\theta = 135$ to 160° ('system R_I'), $\theta = 45°$ ('system B'), $\theta = 0°$ ('system C') and $\theta = 90°$ ('system D'), which is the least conspicuous system of lineaments.

The highest peak in figure 40, in which mean V-values for all 41 test areas are plotted against θ, occurs at 130°, and is a surprisingly strong confirmation that our assumption that the craters

in 'chains' are of internal origin is correct. Furthermore, this peak broadens out to cover exactly the range of azimuth followed by system R_I, that is, the system that is oriented subradially with respect to Mare Imbrium.

The system B peak is present over the range 40 to 50°, but is not as strong as that corresponding to system A, as expected. There is no peak at 0° (system C), but there is a peak at 10° and the departure from 0° may not be important. Lastly, there is a strong, but narrow peak at $\theta = 90°$ (system D). Some small contribution to this peak stemmed from the fact that, in many cases, the boundaries of the individual framelets that were assembled to form a complete Orbiter photograph ran in the direction $\theta = 90°$ and that the picture quality along the joins of framelets was poor in a few of these cases. However, we checked that the 90° peak was real by reference to those photographs which had their framelets oriented at directions of up to 20° from the 90° direction.

It may be argued that there should be no strong correlation between the principal directions of the grid system in the central regions of the lunar disk and our chaining directions, since the latter were measured on photographs drawn from the far side of the Moon and from limb regions as well as from the near side. Most of the test areas are, however, as close to the centre of the Moon's disk as the regions to which the quoted grid directions refer and, thus, the chaining in these areas heavily biases the mean of all chaining directions.

Because of the excellent correlation between the peaks in figure 40 and the independently determined directions of lineaments of the grid system, there can be no doubt that the chains of craters selected by the strip tests are, in general, fracture controlled, and that the craters in question are of endogenic origin.

We sincerely thank Alice Agnieray, L. Betts, D. Clague, A. P. Dawid, J. Denny, Jane Fielder, Dolores Galera, B. Fink, Faye Larson, S. Larson, R. Mitchell, I. Ridpath, and Carla Titulaer for assistance in a variety of ways. Dr A. Marcus read and criticized part of the original manuscript.

We thank the Director of the Steward Observatory, University of Arizona, and R. White for use of the Jarrell–Ash photometer, the Mathematics Department for use of the IBM 1130 Computer and the Computer Centre of the University of Arizona for use of the CDC 6400.

This work was done at the invitation of Dr G. P. Kuiper, Director of the Lunar and Planetary Laboratory, University of Arizona, and was supported by JPL/NASA Contract number 952166. Revisions were completed with the support of NERC Research Grant GR/3/271.

References

Arthur, D. W. G. 1954 The distribution of lunar craters. *J. Br. astr. Ass.* **64**, 127–132.

Arthur, D. W. G., Agnieray, A. P., Horvath, R. A., Wood, C. A. & Chapman, C. R. 1963 The system of lunar craters, quadrant I. *Comm. LPL* **2**, 71–79.

Arthur, D. W. G., Agnieray, A. P., Horvath, R. A., Wood, C. A. & Chapman, C. R. 1964 The system of lunar craters, quadrant II. *Comm. LPL* **3**, 1–3.

Arthur, D. W. G., Agnieray, A. P., Pellicori, R. H., Wood, C. A. & Weller, T. 1965 The system of lunar craters, quadrant III. *Comm. LPL* **3**, 61–64.

Arthur, D. W. G., Pellicori, R. H. & Wood, C. A. 1966 The system of lunar craters, quadrant IV. *Comm. LPL* **5**, 1–2.

Bullard, F. M. 1962 *Volcanoes in history, in theory, in eruption.* University of Texas Press.

Chapman, C. R. 1968 Interpretation of the diameter-frequency relation for lunar craters photographed by Rangers VII, VIII and IX. *Icarus* **8**, 1–22.

Chapman, C. R. & Haefner, R. R. 1967 A critique of methods for analysis of the diameter-frequency relation for craters with special application to the Moon. *J. geophys. Res.* **72**, 549–557.

Fielder, G. 1964 Lunar tectonics. *J. geol. Soc. Lond.* **119**, 65–94.

Fielder, G. 1965 *Lunar geology.* London: Lutterworth Press.

Fielder, G. 1966 Tests for randomness in the distribution of lunar craters. *Mon. Not. R. astr. Soc.* **132**, 413–422.
Fielder, G. & Marcus, A. H. 1967 Further tests for randomness of lunar craters. *Mon. Not. R. astr. Soc.* **136**, 1–10.
Fricker, P. E., Reynolds, R. T. & Summers, A. L. 1967 On the thermal history of the Moon. *J. geophys. Res.* **72**, 2649–2663.
Fryer, R. J. 1968 Crater alignments in the Flamsteed region of the Moon. *Planet. Sp. Sci.* **16**, 809–814.
Guest, J. E. & Fielder, G. 1968 Lunar ring structures and the nature of the maria. *Planet. Sp. Sci.* **16**, 665–673.
Hartmann, W. K. 1967 Lunar crater counts. I. Alphonsus. *Comm. LPL* **6**, 31–38.
Kuiper, G. P. 1967 The lunar surface and the U.S. Ranger programme. *Proc. R. Soc. Lond.* A **296**, 399.
Langley working paper 1967 No. 407, NASA.
McCauley, J. F. 1967 In *Mantles of the Earth and terrestrial planets* (ed. S. K. Runcorn), ch. 8, sect. VIII. London and New York: Interscience Publishers.
Marcus, A. H. 1964 A stochastic model of the formation and survival of lunar craters. I. *Icarus* **3**, 460–472.
Marcus, A. H. 1966*a* A stochastic model of the formation and survival of lunar craters. II. *Icarus* **5**, 165–177.
Marcus, A. H. 1966*b* A stochastic model of the formation and survival of lunar craters. III. *Icarus* **5**, 178–189.
Marcus, A. H. 1966*c* A stochastic model of the formation and survival of lunar craters. V. *Icarus* **5**, 590–605.
Oberbeck, V. R. & Quaide, W. L. 1967 Estimated thickness of a fragmental surface layer of Oceanus Procellarum. *J. geophys. Res.* **72**, 4697–4704.
Strom, R. G. 1964 Analysis of lunar lineaments. I. Tectonic maps of the Moon. *Comm. LPL* **2**, 205–216.
Walker, E. H. 1967 Statistics of impact crater accumulation on the lunar surface exposed to a distribution of impacting bodies. *Icarus* **7**, 233–242.
Vedder, J. F. 1966 Minor objects in the Solar System. *Sp. Sci. Rev.* **6**, 365–414.

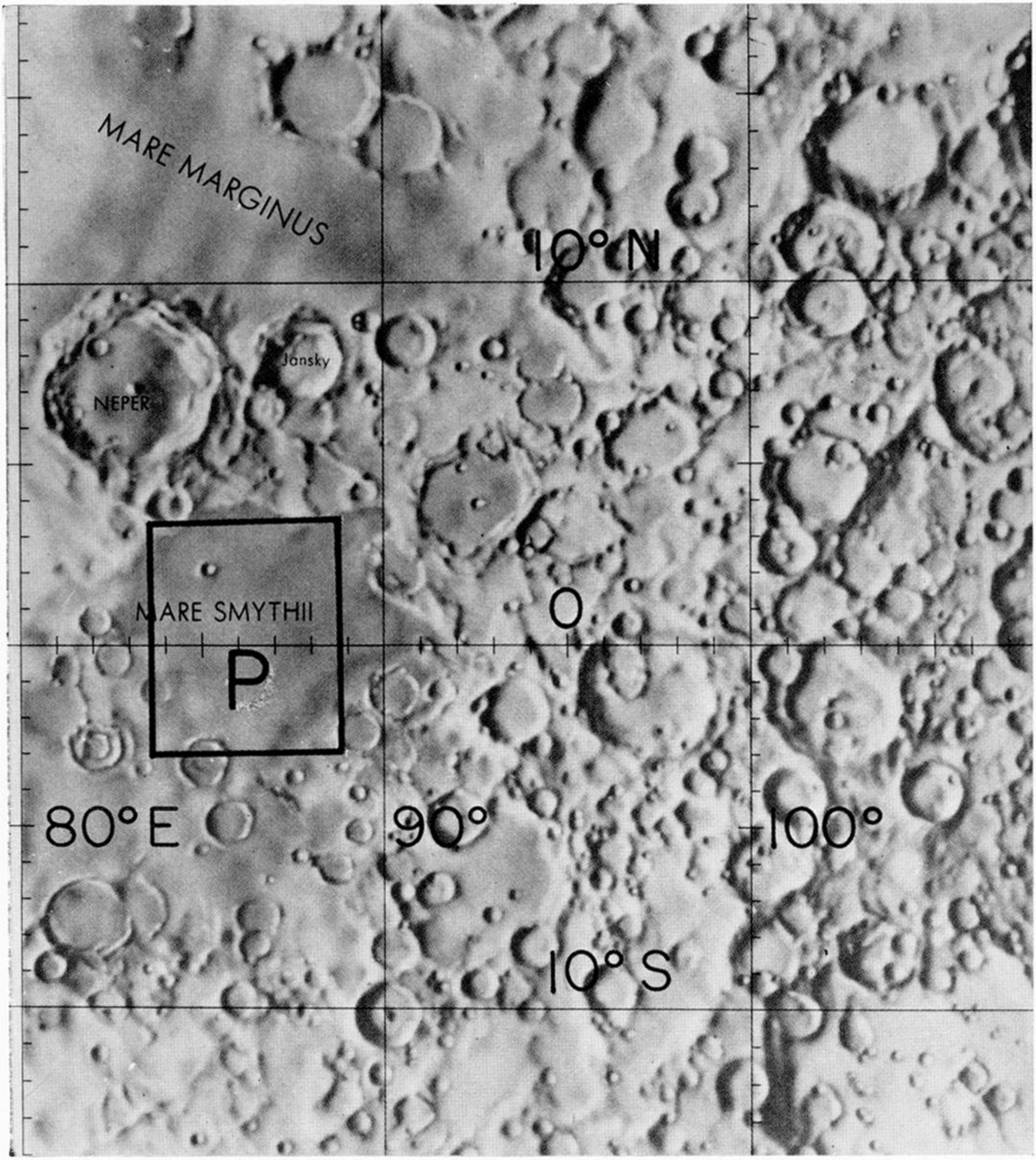

FIGURE 2. Extent of 'area P' in Mare Smythii (limb area).

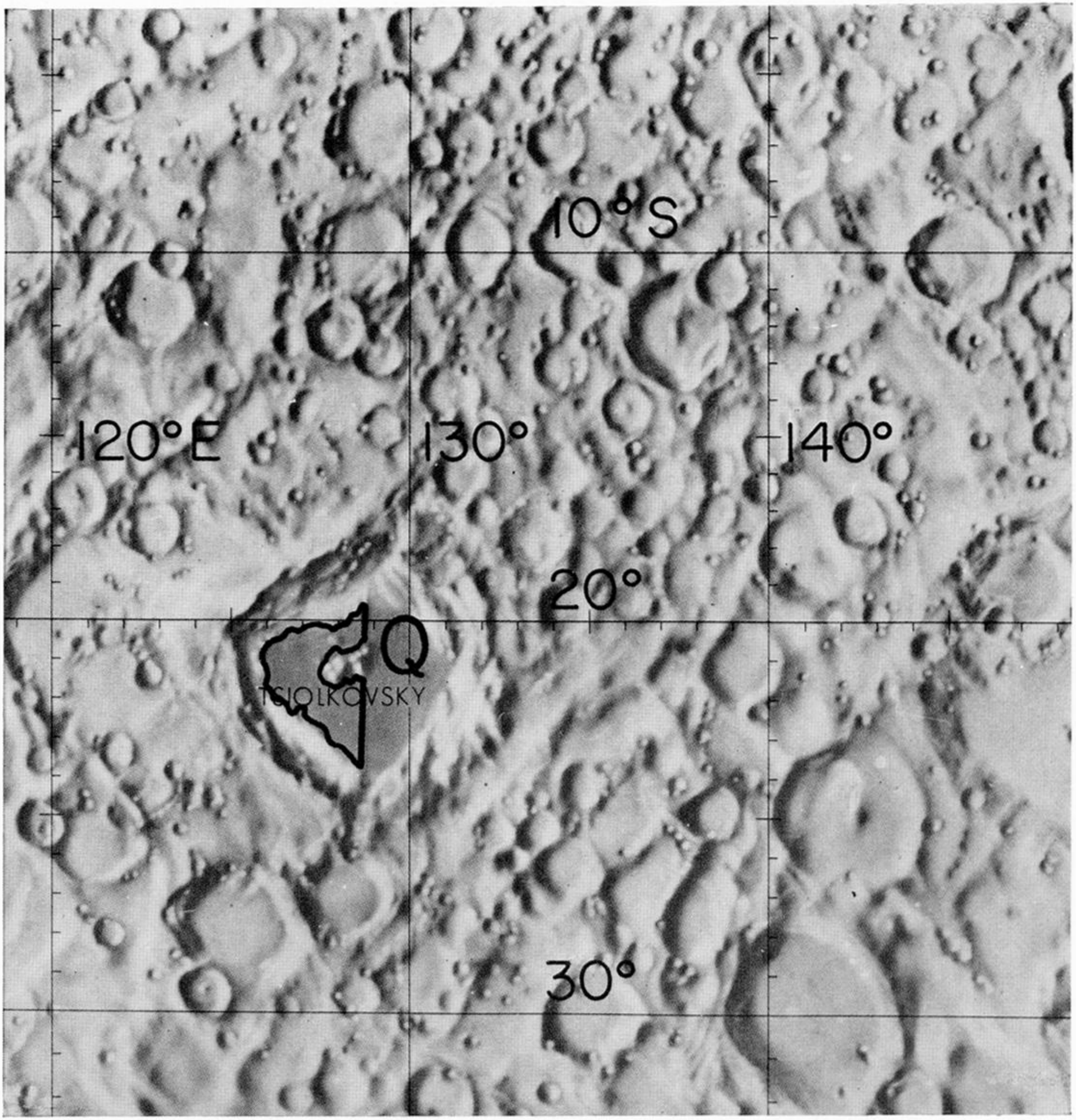

FIGURE 3. Extent of 'area Q' in the large crater Tsiolkovsky (farside of Moon).

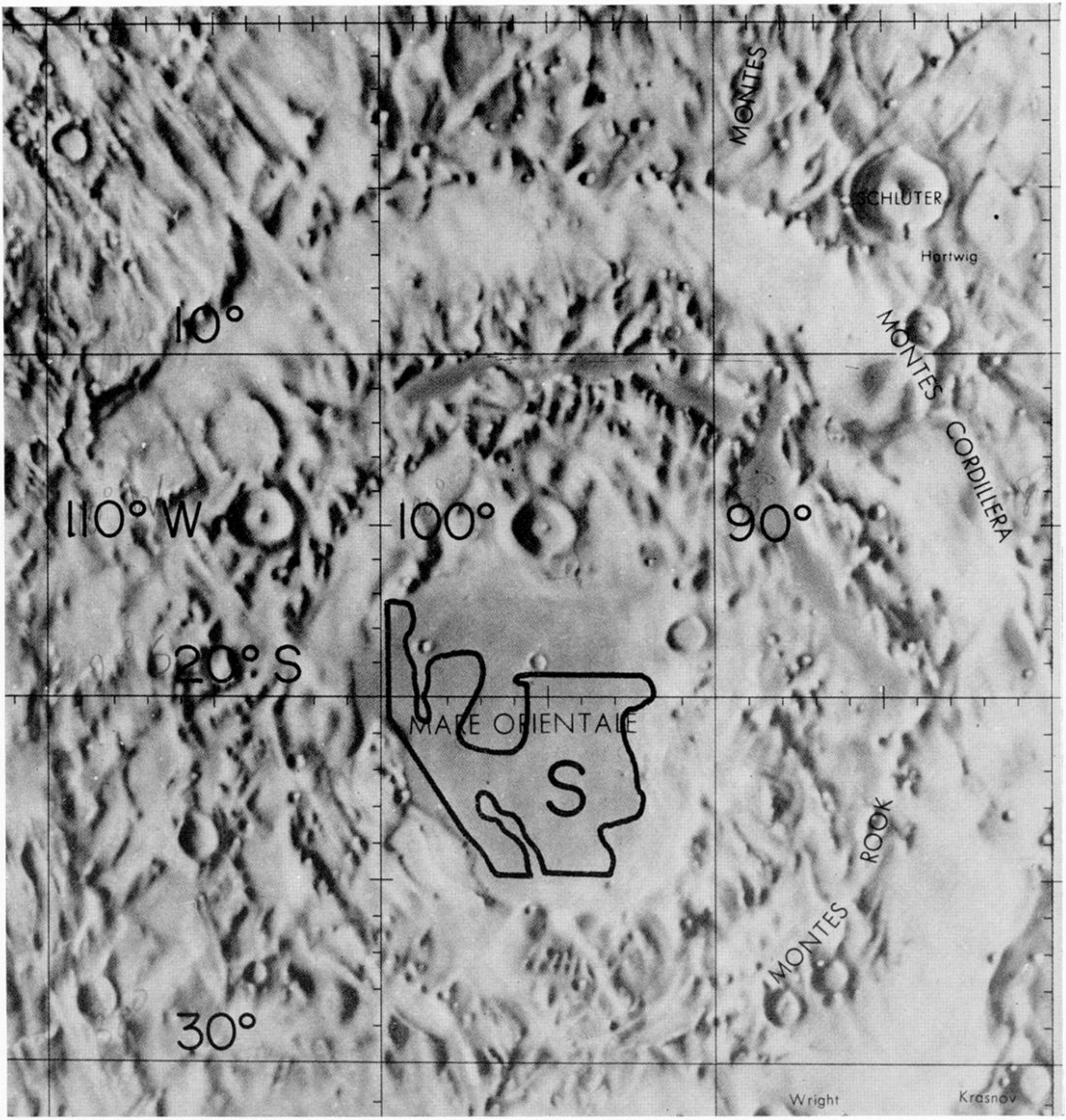

FIGURE 4. Extent of 'area S' in Mare Orientale (limb area).